ADVANCES IN CHEMICAL PHYSICS, VOL. 34
I. Prigogine and Stuart A. Rice
Published by John Wiley & Sons, Inc.

ROLES OF REPULSIVE AND ATTRACTIVE FORCES IN LIQUIDS: THE EQUILIBRIUM THEORY OF CLASSICAL FLUIDS

HANS C. ANDERSEN*

Department of Chemistry,
Stanford University,
Stanford, California

DAVID CHANDLER*

School of Chemical Sciences,
University of Illinois,
Urbana, Illinois

JOHN D. WEEKS

Bell Laboratories,
Murray Hill, New Jersey

CONTENTS

* Alfred P. Sloan Fellow

Abstract

The attractive and the repulsive intermolecular forces play very different roles in forming the equilibrium structure of a dense liquid. The harsh repulsive forces (which fix the *shape* of the molecules) essentially determine the high-density structure. The effect of the attractive forces on the structure can often be ignored or treated by perturbation theory. This idea, which goes back to the time of van der Waals, forms the basis for a quantitative theory of the equilibrium structural and thermodynamic properties of liquids which is reviewed in this article. The structure due to the repulsive forces alone is related to that of the hard sphere model fluid by using an accurate perturbation technique called the "blip function" method. A very simple and accurate theory for the thermodynamic properties of simple dense liquids follows using only the first term in the high-temperature (weak interaction) expansion of the partition function in powers of the attractive interaction.

The effect of the attractive forces on the structure (important at lower density) can be calculated using a generalization of the Mayer cluster theory for ionic solutions called the optimized cluster theory (OCT). By a diagramatic summation, the bare attractive potential is replaced by a renormalized potential. The renormalized potential becomes progressively weaker as the density is increased and the repulsive molecular cores are packed more closely together, thus screening out most of the effects of the attractive forces. A theoretical analysis of the diagrams summed in the OCT as well as numerical results are presented. Some of the implications of these ideas to a number of areas of interest in the liquid state are discussed; for example, the theory of freezing, the static structure of complex molecular liquids and liquid crystals, and dynamical properties of liquids. The relationship between the OCT and the well-known mean-spherical-model integral equation and the diagrams it sums is also given.

I. INTRODUCTION

This article is a review of a theory of liquids that has been developed during the past few years.[1–5] The principal physical concepts and major simplifying feature in this theory originated with the work of van der Waals long ago. It is the idea that for a dense fluid the harsh repulsive forces (which are nearly hard core interactions) dominate the liquid structure. This means the *shape* of molecules determines the intermolecular correlations. Attractive

forces, dipole–dipole interactions, and other slowly varying interactions play a minor role in the structure. Their effect on the thermodynamic properties of a fluid is essentially that of a mean-field or uniform background potential. As a result, if a dense liquid is composed of spherical (or nearly spherical) molecules, the intermolecular structure should be very similar to that of a fluid made up of hard spheres.

In recent years, an important use of the historic van der Waals idea was the theory of freezing developed by Longuet-Higgens and Widom.[6] At about the same time, Reiss[7] concluded on the basis of the scaled particle theory that a liquid has "its volume or density determined by the soft [attractive] part of the intermolecular potential. Once this volume is established one may consider the liquid as a hard sphere fluid confined within it." Other works that were based on the van der Waals concept and set the foundation for the theory reviewed herein are the perturbation theory of liquids developed by Barker and Henderson[8] and Verlet's[9] hard sphere model for the structure of simple liquids.

A qualitative explanation of why the repulsive intermolecular forces dominate the structure of most dense fluids follows from a description of the environment of a particle in a liquid. For simplicity, consider an atomic liquid. The phase diagram is shown in Fig. 1. High density corresponds to thermodynamic states at which $\rho^{-1/3} \lesssim r_0$, where ρ is the average particle density, and r_0 is the location of the minimum in the intermolecular pair potential. A glance at the phase diagram shows that "high density" characterizes most of the liquid phase outside of the critical region. Note that $\rho^{-1/3}$ provides an estimate of the average separation between nearest neighbors. Thus, in a dense liquid, nearest neighbors are crushed extremely close to one another. Any displacement of a particle will cause a large change in the energy associated with the interparticle repulsions. The change in energy associated with the attractions will be relatively small because these interactions are not quickly varying functions of the interparticle separation. As a result, the high-density structure is determined mainly by the repulsive forces.

If the attractions were strong and quickly varying, they too would play an important role in the liquid structure. However, there are few one-component fluids for which this is the case. Liquid water is one of these few exceptions to the van der Waals idea. The hydrogen bond interactions between water molecules are as quickly varying as most of the repulsive forces. Thus, the hydrogen bond plays a crucial role in determining the local tetrahedral arrangement of the water molecules.

Fortunately, the van der Waals idea is correct for nearly all nonhydrogen-bonding dense fluids. In order to demonstrate its quantitative validity, one must be able to calculate the intermolecular correlations that are produced

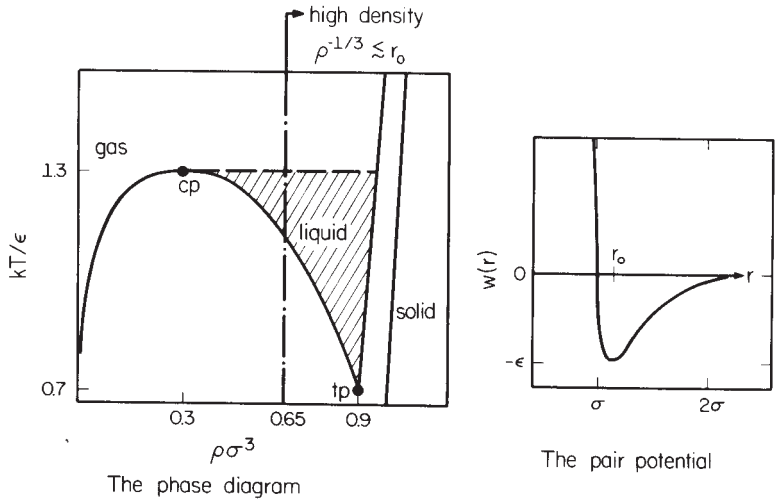

Fig. 1. Phase diagram and intermolecular pair potential for the Lennard–Jones fluid. For particular choices of the length and energy parameters, σ and ε, the Lennard–Jones system is a qualitatively accurate model for several liquids. (See Ref. 23). Notice that the density at the critical point (*cp*) is roughly one third the density at the triple point (*tp*); and the critical temperature is about twice the triple temperature. This approximate scaling holds for nearly all nonhydrogen bonding liquids that are composed of molecules that are relatively small (having $\lesssim 10$ atoms). Thus, the phase diagram shown here is a qualitative representation of the phase diagram for many one-component fluids. The "high-density" region comprises thermodynamic states for which the particle density, ρ, is greater than about twice the critical density, ρ_c.

by the repulsive interactions. This is the subject of Section II where the blip function theory is discussed. The blip function theory is derived by expanding the properties of a general repulsive force system about those of a hard sphere fluid. The theory provides a rigorous relationship between the equilibrium properties of the hard sphere fluid and the properties of fluids with realistic repulsive forces. This produces a major simplification of the classical many-body problem since the configurational properties of the hard sphere fluid are independent of temperature and scale according to one length, the hard sphere diameter. Furthermore, since the properties of the hard sphere system are known from the results of computer simulations,[10] the relationship allows one to calculate equilibrium properties of systems with continuous repulsive forces.

The blip-function method is used in Section III to calculate the equilibrium pair correlation function produced by the repulsive forces in the Lennard–Jones fluid (a model for atomic liquids). The repulsive force structure is then compared with the structure produced by the full Lennard–Jones potential. The comparison demonstrates that at high densities the pair correlations in the Lennard–Jones fluid are indeed dominated by the repulsive forces. The

thermodynamic ramifications of this structural phenomenon are also discussed in Section III.

At low and moderate densities, molecules in a fluid are not very close together, and the attractive forces do play a significant role in the intermolecular structure. A theory to describe the role of attractive forces is discussed in Section IV. The principal procedure in this theory is a rearrangement of the Mayer cluster expansion which allows one to replace the attractive interactions with a renormalized potential.[5] This renormalized (or screened) potential embodies the repulsive force screening which is present in dense fluids. "Repulsive force screening" denotes the mechanism for the reduction of the effect of attractions (and other slowly varying forces) as the density is increased; at high density the particles are so close to one another that the repulsive forces form a structure (essentially due to excluded volume effects) which is not appreciably changed by the attractive interactions. At low densities, repulsive force screening does not exist, and the renormalized potential becomes, in the limit of zero density, the bare attractive interaction.

The principal results obtained from the renormalized cluster expansion are called the optimized cluster theory (OCT). This theory can be used to calculate equilibrium properties of liquids at moderate and low, as well as high, densities. The results of some of these calculations are presented in Section IV.

There are two basic theoretical techniques that are discussed in Sections II through IV. These are the blip function method to describe the effects of repulsive forces, and the OCT to describe the effects of attractions. Together they provide a unified theory for understanding the equilibrium properties of many gases and liquids. However, they are not without limitations. The blip function method is useful only when the molecules in a liquid are fairly spherical. The OCT is reliable only when the density times the renormalized potential is small. The limitations are discussed more fully in Sections II and IV.

There are many important implications to the theory reviewed in this article. They are outlined in Section V. Some of the topics included in the discussion are as follows: the theory of freezing; molecular motion in liquids (i.e., transport coefficients, rotational relaxation times; and time correlation functions); and the static structure of complex molecular liquids.

Appendix A contains a summary of some terminology concerning cluster diagrams. This terminology is used in Section IV. Appendix B presents the diagramatic formulation of the mean-spherical-model integral equation. This equation has been the focus of great interest in recent years and it is intimately related to the theory developed in Section IV.

In closing this Introduction we note four points concerning the format of this article. First, it is not a comprehensive review of all the modern theories of liquids. Rather, the scope is limited to emphasizing the different roles of

repulsive and attractive forces in liquids. For comprehensive reviews the reader is referred to the articles by Barker and Henderson[11] and Andersen.[12] Second, the reader will find that the theory required to describe the role of attractive forces on the liquid structure is inherently more complicated then the formalism needed to describe the effects of the repulsions. Furthermore, the short-ranged harsh repulsions are usually all that one needs to study in order to understand the equilibrium intermolecular structure. For these reasons, the article has been constructed so that Sections II, III, and V can be read independently of Section IV. Third, we consider explicitly simple classical fluids only. However, the theory we present is generalizable to more complex systems. Some applications and extensions of the theory which we will not refer to directly but may be of interest to the reader are the theory of liquid mixtures by Lee and Levesque,[13] studies of molecular fluids by Steele and Sandler[14] and by Sandler et al.,[15] the theory of quantum fluids by Kalos et al.,[16] Shiff's work on astrophysics,[17] and the theory of polar liquids by Stell et al.[18] Finally, we have tried not to simply duplicate the material found in our earlier publications on the blip function expansion and the OCT. Rather, we present in this article relatively different ways of developing those theories. As a result, this review should be regarded as a supplement to Refs. 1–5 and not as a replacement.

II. REPULSIVE FORCES AND THE HARD SPHERE MODEL

Although many workers from the time of van der Waals on realized the the importance of repulsive forces in determining a dense liquid's structure, this insight did not immediately yield a quantitative theory of liquids. It proved very difficult to obtain an accurate description of even the simplest model for a repulsive force system, the hard sphere fluid, so verification and further development of these ideas were not possible.

Thus it is hard to overestimate the importance of the molecular dynamics and Monte Carlo "computer experiments" on the hard sphere fluid which became feasible around 1960[19] and the derivation[20] and the exact solution [21,22] of the Percus–Yevick equation for hard spheres. These gave us for the first time accurate structural and thermodynamic data for a model fluid system over the entire fluid phase. The liquid state was less well understood than the gaseous or solid state primarily because of the lack of a model system, comparable to the ideal gas or the harmonic solid. The modern work on the hard sphere fluid has provided a similarly useful, though necessarily more complicated, starting point for theories of the liquid state.

Analytical formulae are now available which accurately reproduce the results of machine computations on the hard sphere fluid both for the thermodynamic properties and for the pair correlation functions.[10,23] If these hard sphere results are in fact to be useful for quantitative calculations

on real fluids, we must relate the properties of the idealized hard sphere fluid to those of realistic fluids with their smoothly varying repulsive forces. A relationship can be established by considering functional Taylor expansions for the equilibrium properties of a general repulsive force fluid.[4] Articles by Barker[24] and Gubbins et al.[25] provide an alternative approach that could be used to arrive at the same final results [(2.11), (2.16) and (2.17)].

We discuss here the simplest case where the repulsive interactions in the fluid can be represented by "soft sphere" pair potentials $u_R(r)$ which depend only on the scalar distance r between pairs of molecules. Although the smooth $u_R(r)$ may seem to be very different from the discontinuous hard sphere potential $u_d(r)$, which is 0 for $r > d$ and infinite for $r < d$ (their difference being infinite for $r < d$), the thermodynamic and structural properties of both the hard and soft sphere systems are determined by the Mayer cluster functions $f_d(r) = e^{-\beta u_d(r)} - 1$ and $f_R(r) = e^{-\beta u_R(r)} - 1$, respectively, which are very similar to each other [see (2.2) and (2.6)]. Indeed, for a reasonable choice of hard sphere diameter d, the f functions differ from each other only over a small region of space if $u_R(r)$ is a harshly repulsive potential (see Fig. 2). Here $\beta = 1/k_B T$ where T is the temperature, k_B is Boltzmann's constant and the subscript R denotes the soft sphere repulsive force system and d denotes a hard sphere system with diameter d.

We can exploit this similarity by considering a "test system" where the f function $f_\mu(r)$ gradually changes from that of the hard sphere system to that of

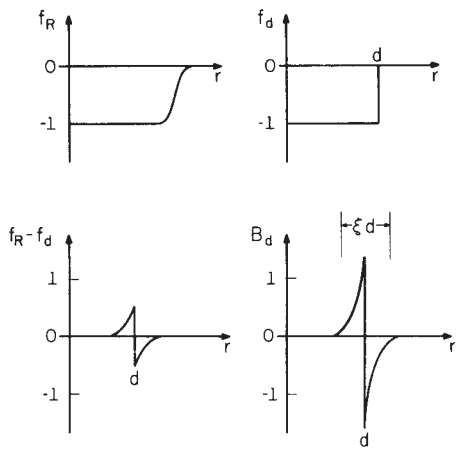

Fig. 2. Schematic plots of some functions considered in the blip function method: (*a*) the Mayer f function for a soft-sphere repulsive potential $f_R(r)$; (*b*) the hard sphere f function $f_d(r)$; (*c*) difference between (*a*) and (*b*); (*d*) blip function $B_d(r)$, showing the significance of the parameter ξ. According to (2.9), the hard sphere diameter d is chosen to make the net area under $r^2 B_d(r)$ equal to zero.

the soft sphere system by means of a coupling parameter μ:

$$f_\mu(r) = f_d(r) + \mu \Delta f(r) \qquad 0 \leq \mu \leq 1$$

where

$$\Delta f(r) = f_R(r) - f_d(r) \tag{2.1}$$

The negative of the dimensionless excess Helmholtz free energy density $\mathscr{A}_\mu$ (with respect to an ideal gas at the same volume V, temperature T, and number density $\rho = N/V$) of a system of N test particles is given by

$$\mathscr{A}_\mu \equiv \frac{-\beta \Delta A_\mu}{V} = V^{-1} \ln Q_\mu \tag{2.2}$$

where

$$Q_\mu = V^{-N} \int \mathbf{dr}^N \prod_{i<j=1}^{N} [1 + f_\mu(r_{ij})] \tag{2.3}$$

Here ΔA_μ is the excess Helmholtz free energy and $\int \mathbf{dr}^N$ denotes an integration over all positions of the N particles in the volume V. Using the familiar coupling parameter technique, we differentiate and then integrate (2.2) with respect to μ and find the exact result

$$\mathscr{A}_R - \mathscr{A}_d = \frac{\rho^2}{2} \int_0^1 d\mu \int \mathbf{dr}\, \Delta f(r) y_\mu(r) \tag{2.4}$$

Here $\mathscr{A}_R$ is the quantity $\mathscr{A}$ for the soft sphere system ($\mu = 1$), $\mathscr{A}_d$ that of the hard sphere system ($\mu = 0$) and

$$y_\mu(r_{12}) = \frac{\dfrac{N(N-1)}{\rho^2} \displaystyle\int \mathbf{dr}^{(N-2)} \prod_{\substack{i<j \\ (i,j)\neq(1,2)}} [1 + f_\mu(r_{ij})]}{\displaystyle\int \mathbf{dr}^N \prod_{i<j} [1 + f_\mu(r_{ij})]} \tag{2.5}$$

Because of the integrations in (2.5), $y_\mu(r)$ is a continuous function of r even when, as in the present case, $f_\mu(r)$ is not. Also $y_\mu(r)$ is positive and is simply related to the pair correlation function $g_\mu(r)$ by

$$[1 + f_\mu(r)] y_\mu(r) = g_\mu(r) \tag{2.6}$$

$g_\mu(r)$ is also called the radial distribution function and is defined so that $4\pi\rho r^2 g_\mu(r)\, dr$ gives the average number of molecules at a distance between r and $r + dr$ from a central molecule.[26]

We anticipate that for a reasonable choice of hard sphere diameter d, the fractional change in $y_\mu(r)$, denoted by

$$\delta y_\mu(r) \equiv \frac{y_\mu(r) - y_d(r)}{y_d(r)} \tag{2.7}$$

will be small. Hence we separate out this fractional change in (2.4):

$$\mathscr{A}_R - \mathscr{A}_d = \frac{\rho^2}{2}\int \mathbf{dr}\, B_d(r) + \frac{\rho^2}{2}\int_0^1 d\mu \int \mathbf{dr}\, B_d(r)\delta y_\mu(r) \tag{2.8}$$

where $B_d(r)$ is the "blip function" given by

$$B_d(r) \equiv y_d(r)\Delta f(r) \tag{2.9}$$

Note that $B_d(r)$, and not simply $\Delta f(r)$, appears naturally. The product $y_d(r)\Delta f(r)$ contains the physical effect of the medium. As the density increases, the medium makes it more likely that a pair of particles will be separated by distances at which $\Delta f(r)$ is nonzero. As a result, the effects of $\Delta f(r)$ grow as the density increases.

Both $\Delta f(r)$ and $B_d(r)$ are nonzero over only a small range of r near $r = d$. Let ξd denote the range of $B_d(r)$. Then the dimensionless parameter ξ can be defined as

$$\begin{aligned}\xi &\equiv \frac{1}{d}\int_0^\infty |B_d(r)|\, dr \\ &\cong \frac{1}{4\pi d^3}\int |B_d(r)|\, \mathbf{dr}\end{aligned} \tag{2.10}$$

For harshly repulsive potentials ξ, the "softness" parameter, is much less than unity (see Fig. 2). It is zero only when the continuous repulsive potential becomes the hard sphere potential.

We want to relate the soft sphere thermodynamic properties to those of a hard sphere system with diameter d chosen to make the correction terms on the right-hand side of (2.8) as small as possible. A particularly appealing choice for d is one that makes the first term, which is apparently of order ξ, vanish. That is, we pick d such that

$$\int B_d(r)\, \mathbf{dr} = \int [e^{-\beta u_R(r)} - e^{-\beta u_d(r)}] y_d(r)\, \mathbf{dr} = 0 \tag{2.11}$$

This is indeed a felicitous choice for d, since we will show that the complicated second term in (2.8) is then of order ξ^4 and thus can frequently be neglected entirely. Furthermore $\delta y_\mu(r)$ is of order ξ^2 with this same choice of d.

To show these facts, differentiate and integrate (2.5) with respect to μ. After integration over irrelevant coordinates the result can be written in the general form

$$y_\mu(r) = y_d(r)\left[1 + \int_0^\mu d\mu' \int \mathbf{ds}\, K_{\mu'}(\mathbf{r}, \mathbf{s}) B_d(s)\right] \tag{2.12}$$

or, using (2.7), and integrating over the angles of **s**,

$$\delta y_\mu(r) = \int_0^\mu d\mu' \int_0^\infty ds\, s^2 \overline{K}_{\mu'}(r, s) B_d(s) \tag{2.13}$$

where

$$\overline{K}_\mu(r, s) = \int_0^\pi \sin\theta_s\, d\theta_s \int_0^{2\pi} d\varphi_s K_\mu(\mathbf{r}, \mathbf{s}) \tag{2.14}$$

Here $\overline{K}_\mu(r, s)$ is a complicated function expressible in terms of integrals over higher-order distribution functions.* Fortunately for the present purposes we need know only some of its general properties. In an isotropic fluid $\overline{K}_\mu(r, s)$ can depend only on the magnitudes of the vectors **r** and **s** since there is no distinguishable direction left after the angular integration in (2.14). This integration also smooths out the jump discontinuities which can occur in the full kernel $K_\mu(\mathbf{r}, \mathbf{s})$ and leaves $\overline{K}_\mu(r, s)$ a continuous function of s. Recalling (2.11), we may rewrite (2.13) as

$$\delta y_\mu(r) = \int_0^\mu d\mu' \int_0^\infty ds\, s^2 [\overline{K}_{\mu'}(r, s) - \overline{K}_{\mu'}(r, d)] B_d(s) \tag{2.15}$$

$B_d(s)$ is nonzero only for a small range of s near $s = d$. This range has width of approximately ξd. In this region the term in square brackets in (2.15) is $0(\xi)$, since $\overline{K}_\mu$ is a continuous function of s. The term $B_d(s)$ provides another factor of $0(\xi)$ in the integrand, by (2.10). Hence δy_μ is $0(\xi^2)$ for all r. Then for $\mu = 1$,

$$y_R(r) = y_d(r)[1 + 0(\xi^2)]$$

or

$$g_R(r) \equiv e^{-\beta u_R(r)} y_R(r) = e^{-\beta u_R(r)} y_d(r)[1 + 0(\xi^2)] \tag{2.16}$$

Similarly, the last term in (2.8) can be written as

$$\frac{\rho^2}{2} \int_0^1 d\mu \int \mathbf{dr}\, B_d(r)[\delta y_\mu(r) - \delta y_\mu(d)]$$

Using the same argument as before, we would expect this integral to be $0(\xi^2)$ if $\delta y_\mu(r)$, like $\overline{K}_\mu(r, s)$, were of order unity. However we have already shown that $\delta y_\mu(r)$ is $0(\xi^2)$. Thus the integral actually is $0(\xi^4)$ and we have

$$\mathscr{A}_R = \mathscr{A}_d + 0(\xi^4) \tag{2.17}$$

Equation (2.11) gives us a criterion for the choice of a temperature- and density-dependent hard sphere diameter d associated with a system of soft

* $K_d(\mathbf{r}, \mathbf{s})$ can be easily derived from the explicit expressions given by Andersen et al.[4]

spheres with potential u_R. Then both the thermodynamics and structure of the soft sphere system can be approximated very simply using (2.16) and (2.17) and the known results for hard sphere systems. The thermodynamic relationship (2.17) is inherently more accurate than the structural one (2.16).

The associated hard sphere diameter d calculated using (2.11) is a decreasing function of temperature and density, in accordance with physical intuition. As the temperature is increased at constant density, the soft sphere molecules have more kinetic energy and can approach each other more closely before finally being repelled by $u_R(r)$. Hence the associated hard sphere diameter decreases. Also when the density is increased at constant temperature, molecules are squeezed closer together so the associated diameter should decrease. The density dependence is much less than the temperature dependence, however.

The correction term of $0(\xi^4)$ to the thermodynamics, given explicitly in (2.8), is also a function of temperature and density and must vanish identically in the low-density limit since $\delta y_\mu(r)$ is $0(\rho)$. The criterion (2.11) assures that (2.17) gives the correct second virial coefficient, and the correct low-density form for $g(r)$ is obtained from (2.16). Thus the lowest-order theory ((2.16) and (2.17)) is exact at low density and when ξ is small should remain accurate even at high density.

Equations (2.16) and (2.17) have been compared to computer "experimental" results for two soft-sphere systems.[4] In the first, $u_R(r)$ is the inverse twelfth-power potential, $\epsilon(\sigma/r)^{12}$ and ξ is rather large ($\xi = 0.35$ at $\rho\sigma^3 = 0.8$ and $k_B T/\epsilon = 1$). In the second, $u_R(r)$ is the repulsive part of the Lennard–Jones potential (see (3.4)) and $\xi = 0.14$ at $\rho\sigma^3 = 0.8$ and $k_B T/\epsilon = 0.8$, so this is a more harshly repulsive potential. For both systems the thermodynamic relationship (2.17) is quantitatively accurate when $\rho d^3 \lesssim 0.93$ (at higher densities the hard sphere fluid is metastable; the hard sphere fluid freezes at $\rho d^3 = 0.93$). ξ is small enough in the repulsive force Lennard–Jones system that both the structural relation (2.16) and the thermodynamic relation (2.17) are very accurate. This system forms the basis of our discussion of the Lennard-Jones liquid in the next section.

When ξ is large, the structural relation (2.16) would be expected to fail at high density. This is the case for the inverse twelfth-power potential,[4,27] and the correction term given in (2.12) is important. We have written down explicitly[4] the correction term to the next order in ξ, which arises when $\bar{K}_\mu(r, s)$ is approximated by $\bar{K}_d(r, s)$ in (2.13). This term can be calculated using presently available data on the hard sphere fluid.[11] This process could in principle be continued with further terms in the Taylor series expansion of $\bar{K}_\mu(r, s)$ about $\mu = 0$ but the additional correction terms require complicated averages over high-order hard sphere distribution functions. What is needed is an approximation for the entire integral over μ in (2.13), that is, a

summation to all orders of ξ of the most important terms in the Taylor series. It may be possible to develop such a theory using the types of techniques to be discussed later in Section IV.

Fortunately, for many applications the correction terms are not needed. Further, when studying particular systems one can determine *a priori* whether the corrections are needed for accurate results. This is done by testing the internal consistency of the simple theory given in (2.16) and (2.17). The thermodynamic properties calculated from (2.17) can be compared with those calculated from (2.16) using the energy or virial equations (see (3.9) and (3.10)). The results of the two separate calculations differ to order ξ^2. If the results agree, then ξ is small enough that both equations are accurate. This has been the case in a number of applications.

The blip function expansion can be easily generalized to multicomponent systems and molecular systems with nonspherical pair potentials, requiring essentially only a change of notation.[28] For example, if the molecular pair potential is of the form $u_R(\mathbf{r}_i, \mathbf{r}_j, \mathbf{\Omega}_i, \mathbf{\Omega}_j)$, where $\mathbf{\Omega}_i$ and $\mathbf{\Omega}_j$ are Euler angles giving the orientation of molecules i and j, then an approximation for the pair correlation function is

$$g_R(\mathbf{r}_i, \mathbf{r}_j, \mathbf{\Omega}_i, \mathbf{\Omega}_j) \cong e^{-\beta u_R(\mathbf{r}_i, \mathbf{r}_j, \mathbf{\Omega}_i, \mathbf{\Omega}_j)} y_d(|\mathbf{r}_i - \mathbf{r}_j|) \tag{2.18}$$

where d is chosen by a generalization of (2.11) which includes an integration over the Euler angles. However, this simple approach is accurate only when the molecules are fairly spherical so that ξ is small.

Thus the blip function method has wide applicability and is very simple to use in practice. In particular it permits us to give a quantitative discussion of the properties of simple liquids, the subject of the next section.

III. ROLE OF REPULSIVE FORCES IN LIQUIDS

Now that we can deal accurately with the repulsive forces in a fluid, we will apply the van der Waals ideas discussed in the Introduction to calculate the thermodynamic and structural properties of realistic fluids, which have attractive as well as repulsive forces.[2,3] As an example, we consider the Lennard–Jones fluids, where the pair potential energy is given by

$$w(r) = 4\epsilon\left[\left(\frac{\sigma}{r}\right)^{12} - \left(\frac{\sigma}{r}\right)^{6}\right] \tag{3.1}$$

Here σ has dimensions of length and ϵ of energy. This model fluids gives a fairly accurate description of the properties of rare gas liquids and has been extensively studied by computer simulations to which we can compare our results.[29,30] The main purpose of this comparison is to gain confidence in the validity of these ideas before applying them to more complicated systems.

A. Separation of the Pair Potential

As discussed in Section I, the structure of a liquid at high density should be determined mainly by the repulsive forces. Thus we separate the intermolecular potential into a *reference* part $u_0(r)$ containing all the repulsive forces and a *perturbation* part $u(r)$ containing all the attractive forces:

$$w(r) = u_0(r) + u(r) \tag{3.2}$$

Note that the force determined from (3.1) is repulsive for all $r < r_0$. Here $r_0 = 2^{1/6}\sigma$ is the distance at which the potential reaches its minimum value. If $u_0(r)$ is to contain all these repulsive forces, no other repulsions and no attractive forces we require

$$\begin{aligned} \frac{du_0(r)}{dr} &= \frac{dw(r)}{dr} \qquad && r \leq r_0 \\ u(r) &= 0 && r > r_0 \end{aligned} \tag{3.3}$$

Equation (3.3) and (3.2) then determine $u_0(r)$ and $u(r)$ uniquely as

$$\begin{aligned} u_0(r) &= w(r) - w(r_0), && r \leq r_0 \\ &= 0, && r > r_0 \end{aligned} \tag{3.4a}$$

and

$$\begin{aligned} u(r) &= w(r_0), && r \leq r_0 \\ &= w(r), && r > r_0 \end{aligned} \tag{3.4b}$$

where $w(r_0) = -\epsilon$ is the minimum value of the potential (3.1). This potential separation is shown in Fig. 3.

With this separation, the physical arguments of Section I suggest that at high densities the effects of the attractive interactions $u(r)$ on the structure

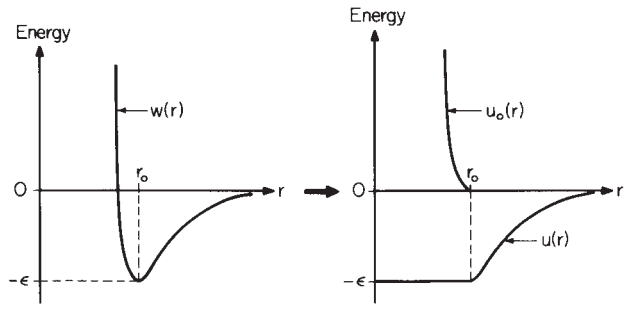

Fig. 3. The unique separation of the Lennard–Jones potential, $w(r)$, into a part $u_0(r)$ containing all the repulsive interactions in $w(r)$ (and no attractions), and a part $u(r)$ containing all the attractive interactions in $w(r)$ (and no repulsions).

of the liquid should be small. In the simplest approximation we ignore them entirely and get

$$g(r) \cong g_0(r) \tag{3.5}$$

Thus the structure of the liquid should be very similar to that of the hypothetical reference fluid which has the same repulsive forces and no attractive forces.

B. Thermodynamic Perturbation Theory

The thermodynamic consequences of this postulated structural behavior are easy to calculate, using coupling parameter methods similar to those in Section II. Consider a "λ system" with pair potential

$$w_\lambda(r) = u_0(r) + \lambda u(r) \qquad 0 \leq \lambda \leq 1 \tag{3.6}$$

Differentiating and integrating the canonical partition function with respect to λ, we find the exact result

$$\mathscr{A} - \mathscr{A}_0 = -\frac{\beta\rho^2}{2} \int_0^1 d\lambda \int \mathbf{dr}\, u(r) g_\lambda(r) \tag{3.7}$$

Here $g_\lambda(r)$ is the pair correlation function when the pair potential is $w_\lambda(r)$, $\mathscr{A}$ is the negative of the dimensionless excess free energy density for the Lennard–Jones system ($\lambda = 1$) and $\mathscr{A}_0$ that for the reference system ($\lambda = 0$). If attractive forces have little effect on the fluid's structure, then $g_\lambda(r) \cong g_0(r)$ and the λ integration in (3.7) is trivial. We then get the high-temperature approximation (HTA),

$$\mathscr{A} \cong \mathscr{A}_0 - \frac{\beta\rho^2}{2} \int \mathbf{dr}\, u(r) g_0(r) \tag{3.8}$$

so named because the attractions would be expected to be of little importance at high enough temperatures. However, the arguments given in the Introduction suggest that (3.5) and hence (3.8) should also be accurate at high density even when the temperature is not high. To test the accuracy of (3.5) and (3.8) one must be able to evaluate $g_0(r)$ and $\mathscr{A}_0$. This is easily done by applying (2.16) and (2.17), respectively, to the Lennard–Jones repulsion $u_0(r)$. The results reported below are calculated in just this way.

Equation (3.8) is usually given as the first term in the high-temperature (weak interaction) series[31,32] which can be derived by expanding $\mathscr{A}$ in powers of the perturbation potential. However, the higher-order terms are so complicated it is difficult to tell whether the weak interaction expansion converges at liquid temperatures or when the first-order result (3.8) will be accurate. The closed expression (3.7) shows it is the effect of the perturbation potential on the liquid's structure that determines the accuracy of the first

approximation (3.8). Thus it is very important to choose a potential separation where $g_0(r) \cong g(r)$ if a simple first-order thermodynamic perturbation theory is to be accurate.

C. Results

Earlier perturbation theories of liquids[8,33] proposed different separations of the potential into reference and perturbation parts. These earlier reference systems differ considerably from the repulsive force reference system, and the perturbation parts contain some strong and rapidly varying forces. As a result, the effect of the perturbation potential on the fluid's structure is large and (3.5) and (3.8) are not accurate for these separations at liquid temperatures and densities.

Figure 4 gives $g(r)$ for the Lennard–Jones liquid at a state near the triple point. This is compared with the $g_0(r)$ for the repulsive force reference system and with the references systems used in the earlier thermodynamic perturbation theories of McQuarrie and Katz[33] ($u_0^{MK}(r) = 4\epsilon(\sigma/r)^{12}$) and Barker and Henderson[8] ($u_0^{BH}(r)$ is the positive part of the Lennard–Jones potential). As expected, (3.5) is a poor approximation in the latter theories and thus large

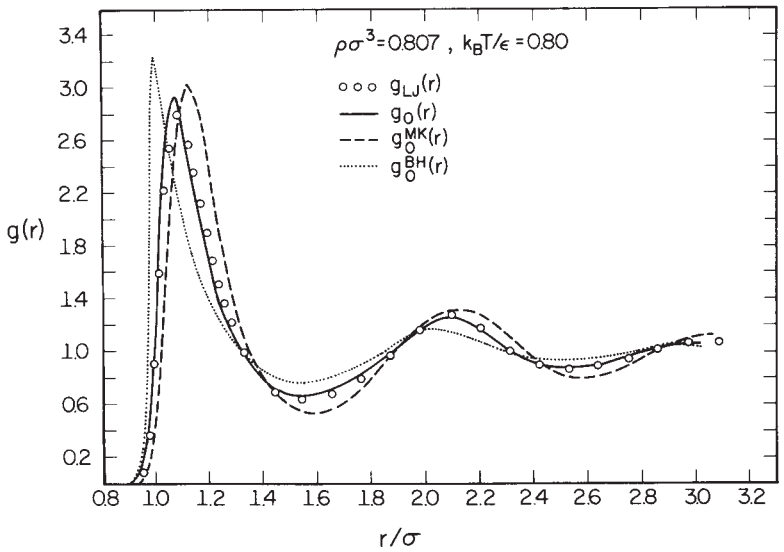

Fig. 4. The Lennard–Jones liquid $g_{LJ}(r)$ at a state near the triple point (calculated using the optimized cluster theory) compared with the repulsive force reference system $g_0(r)$ (calculated using the blip function method) and the correlation functions for the reference systems proposed by Barker and Henderson, $g_0^{BH}(r)$ (calculated using the blip function method), and McQuarrie and Katz, $g_0^{MK}(r)$ (results taken from Monte Carlo calculations of Hansen and Weis[27]). The calculated correlation functions are essentially identical to those that would be given by "exact" Monte Carlo calculations of those functions.

errors result from the use of the HTA ("first-order perturbation theory") for these theories at liquid temperatures and densities.[2,3,10] In contrast, the repulsive force reference system $g_0(r)$ is seen to be very close to the Lennard–Jones $g(r)$. This provides a striking confirmation of the correctness of the physical picture introduced by van der Waals long ago. Figure 4 is typical of the agreement we find between $g(r)$ and $g_0(r)$ for all high-density states.

The main difference between $g_0(r)$ and $g(r)$ is that the first peak in $g(r)$ is moved slightly outward from that of $g_0(r)$. This is easily understood: when attractions are present the neighboring molecules would like to sit in the potential minimum at r_0 for energetic reasons, though only a very small shift is possible because of the packing of the repulsive cores. This small difference in $g(r) - g_0(r)$ is sufficient to cause the use of $g_0(r)$ in the pressure (virial) equation,

$$\frac{\beta P}{\rho} = 1 - \frac{\beta\rho}{6}\int r\frac{dw(r)}{dr}g(r)\,\mathbf{dr} \tag{3.9}$$

to give too large results[10,23] because $dw(r)/dr$ weights the shifted region very heavily. More accurate thermodynamic results arise when $g_0(r)$ is used in the internal energy equation,

$$\frac{\beta\Delta E}{N} = \frac{\beta\rho}{2}\int w(r)g(r)\,\mathbf{dr} \tag{3.10}$$

since $w(r)$ weights the shifted region less strongly than does $dw(r)/dr$. Best of all, however, is the use of the approximation $g_0(r) \cong g_\lambda(r)$ in (3.7) since the smooth $u(r)$ is practically constant over the shifted region. Thus the HTA (3.8) can be very accurate, and quantitative results for the pressure and internal energy of dense liquids can be obtained[3,10,23] by differentiating (3.8) with respect to ρ or β. Table I gives some representative results.

This happy state of affairs extends over that part of the temperature-density plane where (3.5) holds. This includes trivially all high-temperature states ($k_B T/\epsilon \gtrsim 3$) of any density, where $\beta u(r)$ is small, and all high-density states ($\rho\sigma^3 \gtrsim 0.65$) even when the temperature is low and $\beta u(r)$ is large. Thus a large part of the entire phase diagram can be understood using these simple physical ideas, including the dense liquid region where most other approaches have failed.

At lower density and low temperatures and particularly as we approach the critical point the physical ideas suggesting (3.5) and (3.8) no longer hold and we must consider explicitly the effects of the attractive forces on $g(r)$. (This is necessary even at high density if the virial pressures are to be accurate.) The most straightforward approach would be to take the first-order correction to $g_\lambda(r)$ in a power series about $\lambda = 0$, as is done by Barker and Henderson.[11] However, like the μ expansion discussed in Section II, the first-order

TABLE I
Pressure and Internal Energy for the Lennard-Jones Fluid for Several Representative High-Density States Calculated from (3.8)

		$\beta P/\rho$		$-\Delta E/N\epsilon$	
$\rho\sigma^3$	$k_B T/\epsilon$	HTA[a]	MD[b]	HTA[a]	MD[b]
0.88	0.94	2.82	2.77	6.03	6.04
0.85	2.202	4.22	4.20	4.77	4.76
0.85	1.128	2.78	2.78	5.69	5.69
0.85	0.76	0.74	0.82	6.06	6.07
0.75	1.304	1.55	1.61	4.99	5.02
0.75	1.071	0.76	0.89	5.15	5.17
0.75	0.84	0.38	0.37	6.01	6.04
0.65	1.585	1.19	1.25	4.20	4.23

[a] Obtained by numerical differentiation of (3.8).
[b] Molecular dynamics calculations summarized in Verlet and Weis.[10] The uncertainty in these results is ± 0.05.

term in λ for $g_\lambda(r)$ involves complicated averages over three- and four-particle correlation functions, and when $\beta u(r)$ is large, it is not clear why just one more term in λ will be sufficient. In the next section we discuss a renormalization procedure which provides a general treatment of the attractive forces. The renormalization of the perturbation gives us a mathematical basis with which we can understand, in part at least, why the repulsive forces at high density prove so effective in screening out the effects of the attractions. However, before turning to this problem, we consider the relationship between the basic theory described in this section—the HTA—and the van der Waals equation, which in a sense, motivated the present theory.

D. Van der Waals Equation

The van der Waals equation for a one-component fluid is

$$P = P_d - a\rho^2 \tag{3.11}$$

where a is a positive constant and P_d denotes the pressure of the hard sphere fluid. With the appropriate choice for a and d, this equation provides a remarkably accurate description of the equation of state for a dense fluid.*

* Van der Waals actually assumed that $P_d = k_B T\rho(1 - b\rho)^{-1}$, where b is a positive constant which describes the volume of a molecule. This particular form for P_d is correct only for a one-dimensional hard rod fluid. Results are considerably improved when more accurate results for P_d are used. See Widom for an excellent discussion.[34]

This fact can be understood within the framework of the theory developed in this section. By employing (2.16) and (2.17) of the blip function expansion, (3.8) can be expressed as

$$\frac{A}{Nk_BT} \cong \frac{A_d}{Nk_BT} - \frac{\rho a(\rho)}{k_BT} \tag{3.12}$$

where

$$\rho a(\rho) = -\frac{1}{2}\int_d^\infty 4\pi\rho r^2 g_d(r)u(r)\,dr \tag{3.13}$$

The only important approximation involved in this result is the assumption that the structure of the fluid is determined by the repulsive forces. It has been demonstrated that this is an excellent approximation at high densities, i.e., $0.65 \lesssim \rho d^3 \lesssim 0.9$.

Strictly speaking, $a(\rho)$ is also a function of temperature. This arises from the temperature dependence of the hard sphere diameter d. However, for realistic harshly repulsive interactions, d is only a weak function of T. Thus to a good approximation the temperature dependence of $a(\rho)$ can be neglected.

Over the limited region of high density, a linear interpolation of the density dependence of $\rho a(\rho)$ should be fairly accurate, that is,

$$\rho a(\rho) \cong a_0 + \rho a \tag{3.14}$$

where a_0 and a are constants chosen to give the best fit to $\rho a(\rho)$ over the high-density region.* Equation (3.14) may seem even more plausible when one realizes that for short-ranged potentials (such as the Lennard–Jones potential) the major contribution to the integral in (3.13) comes for those values of r in the first coordination shell. Since $4\pi\rho r^2 g_d(r)\,dr$ is the number of hard spheres in a shell between r and $r + dr$ that surround a central hard sphere, the density dependence of the integral in (3.13) is essentially the same as the density dependence of the number of nearest neighbors in a hard sphere fluid. This should vary smoothly with density in the high-density region.

Equations (3.14) and (3.12) can be combined and then differentiated with respect to ρ to yield the pressure. Provided one neglects the density dependence in d (an approximation that is even better than (3.14)), one obtains

$$\frac{\beta P}{\rho} = \frac{\beta P_d}{\rho} - \beta a\rho \tag{3.15}$$

which is van der Waals' equation.

* This choice of the constants a_0 and a may differ considerably from values chosen to fit low-density results. The familiar evaluation of the van der Waals parameters in terms of critical point data[32] is not justified since the HTA and hence the van der Waals equation is not accurate in this low-density regime.

Thus, the basic approximations which justify the van der Waals' equation for real dense fluids are as follows: (1) the structure of the fluid is determined by the repulsive forces; and (2) the number of nearest neighbors to a particle in a dense liquid is approximately a linear function of the density. Approximation (2) is reasonable, but not so accurate as approximation (1).

There exists a well-defined, but certainly unrealistic, class of models for which the van der Waals equation is the exact equation of state.[35] These models are classical fluids for which the total pair potential is $u_d(r) + u_K(r)$, where $u_K(r)$ is a Kac potential. The general form for a Kac potential is

$$u_K(r) = \gamma^v F(\gamma r) \tag{3.16}$$

where v denotes the dimensionality of the system,

$$\int \mathbf{dx}\, F(x) = \alpha \tag{3.17}$$

is a finite constant, and γ tends to zero. Thus, $u_K(r)$ is both infinitely weak and infinitely long ranged. It is intuitively obvious that such a weak and slowly varying interaction will have no effect of the fluid structure, and that its effect on the thermodynamics will be one of a simple mean field or background potential.

To study the effect of $u_K(r)$ mathematically one may start from (3.7). For the model system defined above, we have the exact result:

$$\begin{aligned} \mathscr{A}(T, \rho; u_d + u_K) &= \mathscr{A}_d - \frac{\beta\rho^2}{2} \int_0^1 d\lambda \int \mathbf{dr}\, g_\lambda(r) u_K(r) \\ &= \mathscr{A}_d - \frac{\beta\rho^2}{2}\alpha - \frac{\beta\rho^2}{2} \int_0^1 d\lambda \int \mathbf{dr}[g_\lambda(r) - 1] u_K(r) \end{aligned} \tag{3.18}$$

Since $[g_\lambda(r) - 1]$ decays to zero at large r in a one-phase system, the last integral in (3.18) vanishes as γ tends to zero (this is called the Kac limit). As a result,

$$\mathscr{A}(T, \rho; u_d + u_K) = \mathscr{A}_d - \frac{\beta\rho^2}{2}\alpha \tag{3.19}$$

By differentiating this expression for the free energy one obtains van der Waal's equation with $a = -\alpha/2$ in the one-phase region. In the two-phase region, the thermodynamic properties are obtained by a Maxwell construction.

The Kac potential produces no forces between molecules. As a result, it rigorously has no effect on the fluid structure, and as we have shown, the van der Waals equation is exact for the Kac model. However, this development of the van der Waals equation does not justify the use of the equation

for describing real fluids since the Kac potential is clearly unphysical. The utility of the van der Waals equation arises from the fact that it is a fairly accurate equation even when one considers fluids with realistic pair potentials. In the preceding discussion, we have described the physical reasons for this accuracy.

IV. EFFECT OF ATTRACTIVE FORCES ON LIQUID STRUCTURE

We have seen above that for dense monatomic liquids the structure of the liquid is dominated by the repulsive part of the interatomic potential. The effect of the attractions is much smaller than we might have expected on the basis of the magnitude of the dimensionless parameter, $\epsilon/k_B T$, which characterizes their strength. This is reminiscent of (and, as we shall see below, formally analogous to) the fact that in fluids of charged particles the range and strength of the interparticle correlations is much smaller than we might have expected on the basis of the range and the strength of the Coulomb potential. This latter fact is sometimes called "screening" or "shielding" of the Coulomb potential. Its earliest theoretical description was in the pioneering work of Debye and Hückel[36] on the subject of dilute ionic solutions. They found that although the interionic potential (divided by $k_B T$) for two ions separated by a distance r is approximately

$$\frac{\beta Z_i Z_j e^2}{\epsilon r} \tag{4.1}$$

at large distances, the strength of their correlations (i.e., the pair correlation functions minus unity) is approximately

$$\frac{-\beta Z_i Z_j}{\epsilon} \frac{e^2}{r} e^{-\kappa r} \tag{4.2}$$

Here Z_i and Z_j are the valences of the ions, e is the magnitude of the electronic charge, ϵ is the dielectric constant of the solvent, and κ is the inverse of the "Debye screening length." Its formula is

$$\kappa^2 = \frac{4\pi\beta e^2}{\epsilon} \sum_i Z_i^2 \rho_i \tag{4.3}$$

The exponential factor in (4.2) guarantees that the correlations are weaker and of shorter range than the potential. Mayer[37] extended the work of Debye and Hückel by using the formalism of cluster expansions for fluids. In his theory the function given by (4.2) appears as a screened or renormalized potential energy of interaction among ions. It described a many-body effect which tends to counteract and cancel the direct interactions among the

ions. Some of the Debye–Hückel results were obtained and corrections were expressed in terms of the renormalized potential rather than the original unscreened potential in (4.1). In this section we shall discuss how the ionic cluster theory method of Mayer can be applied to the problem of the structure of dense liquids like the Lennard–Jones fluid. We will define a renormalized potential which plays a role analogous to the Debye–Hückel screened potential. At high densities this renormalized potential is much weaker than the actual attractive potential and seems to describe a many-body screening effect in which the short-ranged repulsive forces tend to counteract and cancel the effect of the attractive forces. We shall call this *repulsive force screening* to distinguish it from the Coulomb screening in ionic solutions.

We will first give a brief review of the cluster theory for the pair correlation function of fluids. The Mayer ionic solution theory will be outlined, including the graphical definition of the screened potential. Then the case of dense fluids will be discussed, showing how the concepts of a renormalized potential can be generalized to cover this situation. The consequences of this for the theory of liquid structure and thermodynamics will then be developed.

A. Cluster Theory of a Fluid of Attracting Hard Spheres

The model fluid of interest has an interatomic potential which is the sum of a hard sphere part plus a perturbation. (We will discuss later the case where there are soft sphere rather than hard sphere repulsive forces.) If $w(r)$ is the interatomic potential, then

$$\begin{aligned} w(r) &= \infty \qquad r < d \\ &= u(r) \qquad r > d \end{aligned} \tag{4.4}$$

where $u(r)$ is the perturbation.

Cluster theories of fluids are often expressed in terms of the Mayer f function for the interaction, defined by

$$\begin{aligned} f(r) &= \exp\left[-\beta w(r)\right] - 1 \\ &= f_d(r) + \left[1 + f_d(r)\right] \sum_{n=1}^{\infty} \frac{1}{n!} (\phi(r))^n \end{aligned} \tag{4.5}$$

where $f_d(r)$ is the Mayer f function for the hard sphere potential, and

$$\phi(r) = -\beta u(r) \tag{4.6}$$

This separation of f into various parts is of use because we expect that in some sense the effect of ϕ on the structure is small compared with the effect of the hard sphere repulsions represented by f_d.

The Mayer cluster theory[38] provides a formula for the pair correlation function of a fluid in terms of an infinite series of diagrams. Each diagram represents an integral whose integration variables represent particle positions and whose integrands contain factors of the Mayer f function of the relative positions of various particles. These diagrams can be expressed in terms of f_d and ϕ, and by a process of topological reduction[38b] they can be expressed in terms of the functions $h_d(r)$ and $\phi(r)$, where

$$h_d(r) = g_d(r) - 1 \tag{4.7}$$

and $g_d(r)$ is the pair correlation function for hard spheres at the density of interest. The resulting expression for $\ln g(r)$ is a convenient starting point for our discussion. It is

$$\ln g(r) = \ln g_d(r) + \text{sum of all connected diagrams with two root points (labeled 1 and 2 and separated by a distance } r\text{), any number of field points, at most one } h_d \text{ bond and any number of } \phi \text{ bonds connecting any two points, at least one } \phi \text{ bond, no articulation points, and no reference pair of articulation points, such that the diagram does not become disconnected if the two roots are removed} \tag{4.8}$$

Appendix A contains a brief review of some of the graph theoretic terms used here. Figure 5 shows various examples of these diagrams. For the present discussion it is necessary to understand only the following features of these diagrams: (*1*) The points 1 and 2 are represented as open circles and should be imagined as being a distance r apart (see Fig. 5). (*2*) The field points are represented as closed circles. (*3*) Each bond in the diagram is represented as a line connecting a pair of points. (*4*) There are two types of bonds, ϕ bonds (represented by solid lines) and h_d bonds (represented by dashed lines). (*5*) The value of each diagram is a certain multidimensional integral over the positions of the field points. (*6*) There is a well-defined prescription for writing down the integral corresponding to any particular diagram.

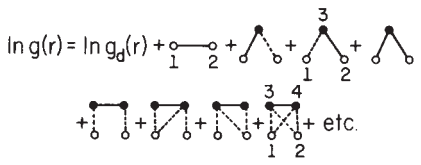

Fig. 5. The first few diagrams in the cluster series [see (4.8)] for the pair correlation function of a model fluid whose intermolecular potential is the sum of a hard sphere part plus a perturbation. Solid lines represent ϕ bonds [see (4.6)], and dashed lines represent h_d bonds [see (4.7)].

Suppose a diagram contains m field points, which are labeled 3, 4, $m + 2$. Then the value of the diagram is

$$\frac{1}{v}\rho^m \int dr_3 \cdots dr_{m+2}\left[\prod h_d(r_{ij})\right]\left[\prod \phi(r_{kl})\right] \tag{4.9}$$

where each h_d or ϕ factor in the integral corresponds to an h_d or ϕ bond in the diagram. Also, v is a numerical factor whose value depends on the topological structure of the diagram. For example the values of the first, third and eighth diagrams in Fig. 5 are, respectively,

$$\phi(r_{12}), \qquad \rho \int \mathbf{dr}_3 h_d(r_{13})\phi(r_{23}),$$

and

$$\tfrac{1}{2}\rho^2 \int \mathbf{dr}_3\, \mathbf{dr}_4 h_d(r_{13})h_d(r_{14})h_d(r_{23})h_d(r_{24})\phi(r_{34}),$$

where $r_{ij} = |\mathbf{r}_i - \mathbf{r}_j|$. For a more detailed discussion of the meaning of the diagrams and for the derivation of (4.8), the reader is referred to Ref. 38.

B. Cluster Theory of Ionic Solutions

Mayer used his cluster theory in a calculation of the properties of a model ionic solution in which the effective interionic interactions are of the type given in (4.1). (An ionic solution should actually be regarded as a two-component fluid since at least two different species of ions must be present to satisfy electroneutrality. This adds some extra complications to the statement of (4.8) and to the definition of the cluster integrals. For simplicity we will ignore these (nonessential) complications in the following discussion of Mayer's derivation of a renormalized potential for ionic solutions.)

The first term in (4.8) for the cluster series for $\ln g - \ln g_d$ represents the contribution from direct Coulombic interaction between the particles. Its value is

$$\phi(r) = \frac{-Z_i Z_j \beta e^2}{\epsilon r} \tag{4.10}$$

and hence it represents a very long-ranged correlation. In the fluid however, the actual correlations are of much shorter range due to a cooperative screening effect. Hence, the sum of the subsequent diagrams in (4.8) must cancel this first diagram for large r. One of the essential features of Mayer's ionic solution theory is that a small subset of these diagrams, rather than the entire sum, can be regarded as responsible for this cancellation. In particular, the diagrams which are simple chains of Coulomb bonds are the

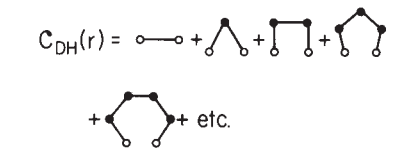

Fig. 6. The first few diagrams in the series for the renormalized potential in the Mayer ionic solution theory. The solid lines are ϕ bonds.

important ones. See Fig. 6, which shows the diagram represented by (4.10) and the chains which cancel it.

The mathematical reason for the cancellation is easy to see if we consider the Fourier transform of the diagrams. The chain diagrams are convolution integrals. For example, the chain of two ϕ bonds is $\rho \int dr_3\, \phi(r_{13})\phi(r_{23})$. The Fourier transform of a convolution is simply a product of the Fourier transforms of the two functions in the integral; hence, the Fourier transform of the diagram is $\rho[\hat{\phi}(k)]^2$, where

$$\hat{\phi}(k) = \int \mathbf{dr}\, e^{\mathbf{ik}\cdot\mathbf{r}}\phi(r) \tag{4.11}$$

Similarly the Fourier transform of the chain with n ϕ bonds is

$$\rho^{n-1}[\hat{\phi}(k)]^n \tag{4.12}$$

The sum of the chains of two or more ϕ bonds is a geometric series whose sum is

$$\hat{\phi}(k)\left[\frac{\rho\hat{\phi}(k)}{1-\rho\hat{\phi}(k)}\right] \tag{4.13}$$

The long-ranged nature of the Coulomb potential is displayed in the Fourier transform of $\phi(r)$ as a divergence of $\hat{\phi}(k)$ for small k, that is,

$$\hat{\phi}(k) \sim \frac{-1}{k^2} \tag{4.14}$$

for small k. It is easily seen from (4.13) that as $k \to 0$ the factor in square brackets approaches -1, and thus the sum of chains of two or more ϕ bonds approaches $-\hat{\phi}(k)$ as $k \to 0$. This exactly cancels the divergence of the Fourier transform of the first diagram in the cluster series and hence exactly cancels the long-range nature of the diagram. $\hat{C}_{DH}(k)$, the sum of all the chains including the first diagram in the series, is given by

$$\hat{C}_{DH}(k) = \hat{\phi}(k)[1-\rho\hat{\phi}(k)]^{-1} \tag{4.15}$$

which leads to the Debye–Hückel potential in (4.2) upon Fourier inversion. (Here the subscript DH denotes Debye–Hückel). An extra advantage of

adding these terms together is that it cancels the divergence in each of the chain diagrams [see (4.12) and (4.14)]. In fact, the chains with two or more links are represented by divergent integrals, but the sum of chains is a finite quantity. Thus far, we have

$$\ln g(r) = \ln g_d(r) + C_{DH}(r) + \text{sum of all diagrams in (4.8) which are not chains of } \phi \text{ bonds} \tag{4.16}$$

At this stage, even though the cancellation of the long-range part of ϕ and the cancellation of the divergences in the chain diagrams are explicitly contained in the results, (4.16) is unsatisfactory because there remain many divergent integrals among the diagrams left. The next important feature of Mayer's theory is that these remaining divergences also cancel each other. This can be shown by expressing the sum of all the remaining diagrams in terms of C_{DH} rather than ϕ. The result can be expressed as follows:

$$\ln g(r) = \ln g_d(r) + \text{sum of all connected diagrams with two root points (labeled 1 and 2 and separated by a distance } r\text{), any number of field points, at most one } h_d \text{ bond and any number of } C_{DH} \text{ bonds connecting any two points, at least one } C_{DH} \text{ bond, no articulation points, no reference pair of articulation points, such that the diagram does not become disconnected if the two roots are removed, and such that no field point has two } C_{DH} \text{ bonds and no } h_d \text{ bonds attached to it.} \tag{4.17}$$

The first few diagrams in this series are shown in Fig. 7. Just as the first diagram in Fig. 7 is the sum of chains of one or more ϕ bonds, in the same way every other diagram in Fig. 7 or (4.17) is the sum of an infinite number of diagrams in Fig. 5 or (4.8); for example, see Fig. 8. The fact that each diagram in (4.17) is expressed in terms of C_{DH} bonds rather than ϕ bonds shows that

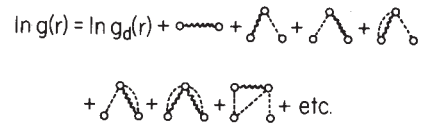

Fig. 7. The first few diagrams in the renormalized cluster series [see (4.17)] for the pair correlation function of an ionic solution. Wavy lines are C_{DH} bonds and dashed lines are h_d bonds.

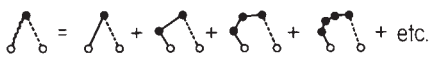

Fig. 8. The second diagram in Fig. 7 is the sum of an infinite number of diagrams in Fig. 5.

the long-ranged divergences of the diagram in (4.8) completely cancel one another. $C_{\mathrm{DH}}(r)$ is sometimes called a "renormalized potential" since it enters the series in (4.17) in much the same way as ϕ enters (4.8).

Equation (4.17) is a good starting point for numerical calculations of the properties of ionic solutions, particularly for low concentrations of singly charged ions. Under these conditions

$$g_d(r) \cong e^{-\beta u_d(r)} \tag{4.18}$$

and to lowest order in the density only the $C_{\mathrm{DH}}(r)$ diagram in (4.17) needs to be retained. The result is

$$g(r) = e^{-\beta u_d(r)} e^{C_{\mathrm{DH}}(r)} \tag{4.19}$$

which is a nonlinear Debye–Hückel result.

We can summarize the major ideas of the Mayer ionic cluster theory in the following way: There is a cooperative screening effect in ionic solutions in which those correlations between two ions which are induced by their direct interaction is screened by the presence of other ions. A mathematical representation of the screening shows that the cluster diagram involving only the direct interaction of two ions is largely canceled by a set of other diagrams which have the topological structure of chains. The sum of the direct interaction and these chains is defined as the renormalized potential. The fact that the renormalized potential is of shorter range and is weaker than the direct interaction is a manifestation of this cancellation or screening. Furthermore the renormalized potential can be used to eliminate the original potential from the cluster series, thus showing that the cancellation and the elimination of divergences extends to all terms in the cluster series and is not confined just to the specific diagrams in the renormalized potential. It is this feature of the renormalization method that distinguishes it from other *ad hoc* truncations of cluster expansions, such as are suggested by various integral equations for the pair correlation function. The resulting series is an expansion in powers of the renormalized potential, rather than the Coulomb potential, and is much more suitable for numerical evaluation.

C. Comments about the Renormalization Technique

There are several important points about Mayer's renormalization techniques which merit further discussion. We do not know the relationship between the physical nature of the Coulomb screening effect and the topological structure (chains of ϕ bonds) of the diagrams chosen to be in the renormalized potential. This is unfortunate since a proper coupling of physical intuition with the mathematics of cluster expansions would be of enormous help in extending the theory of different types of fluids. Since Mayer's choice cannot be justified on physical grounds we must be satisfied

with the mathematical justification discussed above; with this choice all the divergences of the diagrams due to the long-range nature of the potential are systematically eliminated. Moreover the resulting series is useful for numerical calculations and leads to the experimentally verified Debye–Hückel limiting laws for the thermodynamic properties of dilute ionic solutions. However, Mayer's is by no means the only choice yielding these desirable properties and in the next section we will consider other possible choices which are more appropriate for dense fluids.

D. Cluster Theory of Dense Fluids

In this section we will discuss a way of generalizing Mayer's renormalized potential to the case of dense liquids. For dense liquids of molecules interacting with slowly varying long-ranged forces, for example, the Kac model potential, one form of renormalized potential that has been suggested is a sum of chains of not only ϕ bonds but also h_s bonds, where h_s is the "short-ranged part" of h.[39–41] The simplest choice for h_s is h_d.[42] Using it, we define

$$C_K(r) = \text{sum of all diagrams in (4.8) for ln } g(r) \text{ which are chains of } \phi \text{ bonds and } h_d \text{ bonds.} \tag{4.20}$$

Here K stands for Kac. Each member of the series contains at least one ϕ bond, and, as a result of one of the topological restrictions in (4.8), no two adjacent members of the chain can both be h_d bonds. See Fig. 9 for the first few diagrams in the series. These diagrams include all those in Mayer's definition, plus additional ones which describe the effect of the hard sphere forces.

These diagrams are all convolution integrals and their sum can be readily evaluated using Fourier transform techniques. The result is

$$\hat{C}_K(k) = \frac{\hat{S}_d(k)\hat{\phi}(k)\hat{S}_d(k)}{[1 - \rho\hat{S}_d(k)\hat{\phi}(k)]} \tag{4.21}$$

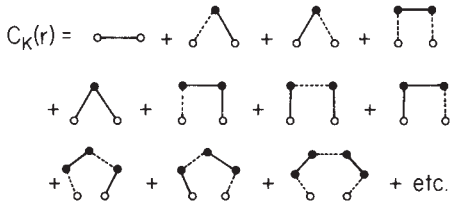

Fig. 9. The first few diagrams in the definition [see (4.20)] of the renormalized potential for the Kac model fluid. Solid lines are ϕ bonds and dashed lines are h_d bonds.

where

$$\hat{S}_d(k) = 1 + \rho \int \mathbf{dr}\, e^{i\mathbf{k}\cdot\mathbf{r}}(g_d(r) - 1) \tag{4.22}$$

$\hat{S}_d(k)$ is called the structure factor of the hard sphere fluid. It is real and positive for all values of $\mathbf{k}$ and depends only on the magnitude of $\mathbf{k}$. This renormalized potential, like Mayer's, has the property that even if $\hat{\phi}(k)$ diverges as $-1/k^2$ for small k, the renormalized $\hat{C}_K(k)$ approaches a finite value, $-\hat{S}_d(0)$, as $k \to 0$. Thus in Fig. 9, the first diagram is to some extent cancelled by the others.

When this new renormalized potential is used for high-density fluids, the possibility of a new type of divergence arises. Namely, if $\hat{\phi}(k)$ is positive for some value of k and if ρ is large enough, we might have

$$\rho\hat{S}_d(k)\hat{\phi}(k) = 1 \tag{4.23}$$

for some particular k, which leads to a divergence in $\hat{C}_K(k)$. This breakdown of the renormalized potential is sometimes misinterpreted as a breakdown of the fluid, that is, the onset of instability or a phase transition. In fact it is just an artifact of this particular choice of diagrams in (4.20). This divergence must be eliminated in order for the renormalized potential to be useful. One method of doing this is to make a better choice of h_s than h_d in the chain sum (4.20).[43–45] Another method is discussed by Andersen and Chandler[5] and leads to the theory called the optimized cluster theory. Here we will discuss a third method which involves finding those diagrams in (4.8) that cancel the divergence and including these additional diagrams in the definition of the renormalized potential. The results obtained are equivalent to those developed in the original formulation of the optimized cluster theory.

To find a set of diagrams that cancel the divergence in C_K, consider those graphs that can be described in the following way (see Fig. 10): Imagine the two root points and a set of one or more field points located on the circumference of a circle, so that by passing from root 1 and going clockwise around

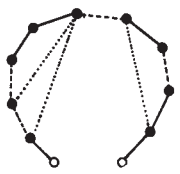

Fig. 10. Illustration for the definition of the diagrams in $C_L(r)$, the renormalized potential appropriate for liquids. The points are on a circle, with a chain of $\phi + f_d\phi = \Phi$ bonds (represented by solid lines) and h_d bonds (represented by dashed lines) leading from one root to another. There are f_d bonds (represented by dotted lines) connecting some pairs of points.

the circle one passes through all the field points and then arrives at 2. Now imagine connecting each pair of adjacent points on this circle with either an h_d bond or a Φ bond, where

$$\Phi(r) = [1 + f_d(r)]\phi(r) \tag{4.24}$$

except that no such bond is to connect the roots directly. This generates a chain similar to, and in many cases identical with, the chains in C_K. However, now we are using Φ bonds rather than ϕ bonds. The former are "decorations" of the latter. Every diagram that is expressed with n Φ bonds is equal to a sum of 2^n diagrams expressed with ϕ and $f_d\phi$ bonds. These decorations prohibit the overlap of two particles which are directly connected by a ϕ bond since $1 + f_d(r)$ is zero for $r < d$. [Outside the hard core, of course, $\Phi(r) = \phi(r)$].

Overlap of nonadjacent particles in the diagrams should also be inhibited (if not prohibited). Thus further decorations are also required. The ones we consider are reminiscent of the cluster diagrams contributing to the Percus–Yevick equation for $y_d(r)$.[46] Imagine adding some or no f_d bonds between nonadjacent points on the circle in such a way that no two f_d bonds cross each other and so that no field point is left with only h_d bonds attached to it. An f_d bond may or may not be drawn between the roots.

Our new definition of the renormalized potential, which we call $C_L(r)$, is that it includes the diagram with just one Φ bond between the roots plus all the diagrams that can be drawn in the way just described. Some examples of the diagrams in C_L are shown in Fig. 11. This renormalized potential is given the subscript L because it is a very useful one for liquids. Some examples of diagrams not in C_L are shown in Fig. 12. Each diagram in C_L contains at least one Φ bond and has no reference pair of articulation points. Also note

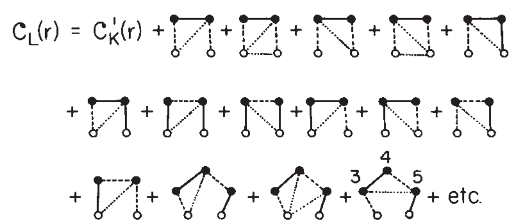

Fig. 11. Diagrammatic equation for the renormalized potential for liquids. The quantity $C_K'(r)$ is the sum of all diagrams in $C_K(r)$ (see Fig. 9) except the ϕ bonds are replaced by Φ bonds ($\Phi = \phi + f_d\phi$). The solid lines are Φ bonds. The dashed lines are h_d bonds. The dotted lines are f_d bonds. The first four diagrams represent ways of decorating the fourth diagram in Fig. 9. The next six represent ways of decorating the sixth, seventh, and eighth diagrams of Fig. 9. The next two are included in $C_L(r)$ even though they are not decorated versions of a diagram in $C_K(r)$. The last three are some of the ways of decorating the ninth diagram in C_K.

Fig. 12. Diagrams which are not included in the definition of $C_L(r)$. The first diagram is excluded because it has crossing f_d bonds. If one or both of these bonds are removed, the diagram becomes acceptable. The next two are excluded because each has one point with only h_d bonds attached.

that for each diagram in C_L with one or more field points which does not have an f_d bond between the roots, there is another diagram in C_L which is identical except for the presence of an f_d bond between the roots, and vice versa. It follows that

$$C_L(r) = 0 \qquad \text{for } r < d \tag{4.25}$$

since

$$f_d(r) = -1 \qquad \text{for } r < d \tag{4.26}$$

and hence each such pair of diagrams is equal in magnitude but opposite in sign for $r < d$.

This choice of renormalized potential includes all the diagrams in $C_K(r)$. Moreover, we will show that it includes diagrams which cancel the divergence in $C_K(r)$. (These extra diagrams, containing f_d bonds, are obtained by breaking up the corresponding diagrams in (4.8).) Hence it is a more suitable choice of renormalized potential for dense liquids at low temperatures. Not only is it suitable, it is also very useful and leads to an accurate theory of the structure of simple liquids, as we shall see below.

We must now find a way of adding these diagrams. Let us note that some of the diagrams in C_L (i.e., all except for the first diagram $\Phi(r)$ and the diagrams with an f_d between the roots) have nodal points, that is, field points which if removed would disconnect the diagram into two parts, with one root point in each part. For example, in the first diagram in Fig. 11, the field point on the right is a nodal point. Let $\psi(r)$ be the sum of the diagrams in $C_L(r)$ with nodal points and let $\phi'(r)$ be the sum of all the nodeless diagrams. Then, obviously

$$C_L(r) = \phi'(r) + \psi(r)$$

Moreover, from the remarks above we have the following relationship:

$$\phi'(r) = \Phi(r) + f_d\psi(r) \tag{4.27}$$

because every nodeless diagram with one or more field points has the structure of a nodal diagram with an f_d bond added between the roots. Next, note that all the diagrams in C_L may be regarded as chains, with the links in the

chains being joined at nodal points. There are three types of links: h_d, $(1 + f_d)\phi = \Phi$, and f_d times a member of the series for ψ. For example, the last diagram shown in Fig. 11 has two nodal points, 3 and 5, and may be regarded as a chain of three links. The first link, connecting 1 and 3, is h_d. The third link, connecting 5 and 2, is Φ. The second link, connecting 3 and 5, is a product $f_d(r_{35})$ and a nodal diagram. This nodal diagram is included in $C_L(r)$ and is shown explicitly as the third diagram on the right side of the equation in Fig. 9. The only restriction on these chains is that no h_d links can be attached together. Then the general diagram in $C_L(r)$ is a chain whose links are h_d bonds and members of the series defining $\phi'(r)$ with the additional restriction mentioned above. Topologically, the series for $C_L(r)$ is similar in structure to $C_K(r)$, and we can use (4.21) to obtain the result

$$\hat{C}_L(k) = \frac{\hat{S}_d(k)\hat{\phi}'(k)\hat{S}_d(k)}{[1 - \rho\hat{S}_d(k)\hat{\phi}'(k)]} \tag{4.28}$$

Note that this is not a solution for $\hat{C}_L(k)$ but actually an integral equation, since $\phi'(k)$ on the right side is defined in terms of the diagrammatic structure of $C_L(r)$ in (4.27).

To solve this integral equation we will use a variational method. Let us define the following functional of ϕ':

$$F(\phi') = \frac{1}{(2\pi)^3\rho}\int \mathbf{dk}\{\rho\hat{S}_d(k)\hat{\phi}'(k) + \ln[1 - \rho\hat{S}(k)\hat{\phi}'(k)]\} \tag{4.29}$$

If we take the functional derivative of $F(\phi')$ with respect to $\hat{\phi}'(k)$ we obtain

$$(2\pi)^3\frac{\delta F(\phi')}{\delta\hat{\phi}'(k)} = -\frac{\rho\hat{S}_d(k)\hat{\phi}'(k)\hat{S}_d(k)}{[1 - \rho\hat{S}_d(k)\hat{\phi}'(k)]} = -\rho\hat{C}_L(k) \tag{4.30}$$

from (4.28). This leads to

$$\frac{\delta F(\phi')}{\delta\phi'(r)} = -\rho C_L(r) \tag{4.31}$$

To use these results, note that from (4.27) we have

$$\phi'(r) = -\beta u(r) \qquad r \geq d$$

and

$$\phi'(r) = -\psi(r) \qquad r < d$$

and from (4.25) that

$$C_L(r) = 0 \qquad r < d$$

If we regard $\phi'(r)$ for $r < d$ as the quantity to be calculated we see from (4.31) and (4.25) that the behavior of $\phi'(r)$ for $r < d$ is such as to make $F(\phi')$ stationary with respect to changes in $\phi'(r)$ for $r < d$. Moreover, since

$$x + \ln(1 - x) \geq 0 \qquad \text{for all } x < 1 \tag{4.32}$$

we have

$$F(\phi') > 0 \tag{4.33}$$

for all ϕ' for which the integral exists. Hence if we imagine choosing $\phi'(r)$ for $r > d$ according to (4.27) and then varying $\phi'(r)$ for $r < d$ so as to minimize $F(\phi')$, at the minimum F will be stationary. Hence to sum the diagrams in $C_L(r)$ we must find the function $\phi'(r)$ for $r < d$ which minimizes $F(\phi')$. When $\phi'(r)$ is substituted into (4.28), we can obtain $\hat{C}_L(k)$ and by Fourier inversion obtain $C_L(r)$.

The process of minimizing $F(\phi')$ is a straightforward one to perform numerically. One way this can be done is to use a trial solution of the form

$$\begin{aligned} \phi'(r) &= \sum_{n=0}^{m} a_n \left[1 - \left(\frac{r}{d}\right)\right]^n \qquad && \text{for } r < d \\ &= -\beta u(r) && \text{for } r > d \end{aligned} \tag{4.34}$$

and minimize $F(\phi')$ with respect to the coefficients $a_0, \ldots, a_m$ by a Newton–Raphson method.[47]

Now let us use this variational principle to discuss the nature of the renormalized potential, $C_L(r)$. We will show that $C_L(r)$ has no divergence of the type which occurs in $C_K(r)$. Moreover, we will see that at high densities, the first term in C_L, namely $\Phi(r)$, is largely canceled by the sum of the remaining terms. This is a mathematical representation of repulsive force screening, that is, of the fact that at high density the structure of a simple liquid is not greatly affected by the attractive forces.

To discuss this divergence, let us consider the integral in (4.29) for F that attains its minimum value when evaluated using the actual behavior of $\phi'(r)$ for $r < d$. The integrand is positive definite and is small only if $\rho\hat{S}_d(k)\hat{\phi}'(k)$ is small. In the variational calculation, $\phi'(r)$ will assume the functional form necessary to make $\rho\hat{S}_d(k)\hat{\phi}'(k)$ as small as possible for all values of k. Moreover, it will especially try to avoid the singularity associated with having $\rho\hat{S}_d(k)\hat{\phi}'(k) = 1$ for any value of k. We might expect, therefore, that

$$\rho\hat{S}_d(k)\hat{\phi}'(k) < 1 \tag{4.35}$$

for all values of k, as has been checked in several numerical tests of the minimization procedure for various model fluids. This means that the renormalized potential $C_L(r)$ contains no divergences, and so the singularities in $C_K(r)$ are canceled by the additional diagrams included in the definition of $C_L(r)$.

From the diagramatic definition of C_L (see Fig. 11), it is seen that at low density

$$C_L(r) = -\beta u(r) + 0(\rho) \qquad r > d \tag{4.36}$$

that is, at low density the renormalized potential is the same as the actual perturbation potential.* [This result can also be easily verified using the low-density limit of the variational procedure given in (4.34)]. At higher densities, however, the minimization procedure tends to make $\rho\hat{S}_d(k)\hat{\phi}'(k)$ as small as possible. From (4.28) it can be seen that this makes $\hat{C}_L(k)$ small. The actual $\hat{\phi}(k)$, therefore, tends to be small for values of k where $\hat{S}_d(k)$ is large, and if necessary to achieve this, it is allowed to become large where $\hat{S}_d(k)$ is small. At low densities, $S_d(k)$ is approximately unity for all k and we obtain (4.36). At high density, $S_d(k)$ is very small for small k, that is, for $k \lesssim \pi/d$. This gives ϕ' some added flexibility in its attempt to minimize $F(\phi')$. The net result is that the renormalized potential is smaller at high density than at low density and hence actually decreases as ρ increases. This is the repulsive force screening effect mentioned above: for example, see Fig. 13, which shows $C_L(r)$ for various densities at the same temperature. The potential used in the calculations is a hard sphere potential plus an attractive perturbation of the Lennard–Jones type. It can be seen that as the density is increased the renormalized potential decreases in magnitude.

We have defined the renormalized potential as the sum of a subset of the diagrams in the original cluster series (4.8) for ln g. An important consequence of this particular definition of $C_L(r)$ is that the entire series for ln g can be expressed in terms of C_L. The details of this topological reduction are straightforward and will be omitted. The result is

$$\ln g(r) = \ln g_d(r) + C_L(r) + \text{sum of all connected diagrams with two root points (labeled 1 and 2 and separated by a distance } r\text{), at least one field point, at most one } h_d \text{ bond and any number of } C_L \text{ bonds connecting any two points, no articulation points, no reference pair of articulation points, no field point with only a } C_L \text{ bond and an } h_d \text{ bond or only two } C_L \text{ bonds attached to it, such that the diagram does not become disconnected if the two roots are removed.} \tag{4.37}$$

* For ionic solutions at low density we find that

$$\begin{aligned} C_L(r) &= C_{\mathrm{DH}}(r) + O(\rho) \qquad r > d \\ &= 0 \qquad\qquad\qquad\quad r < d \end{aligned}$$

so this method reduces to Mayer's under these conditions.

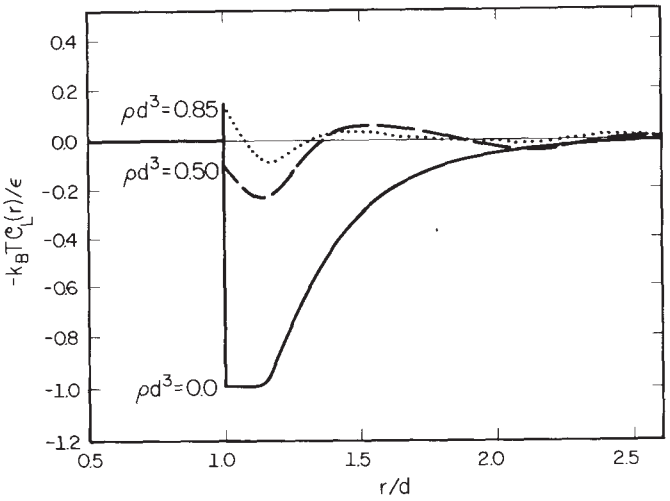

Fig. 13. Renormalized potential at three representative states for the system for whicl $w(r) = u_d(r) + u(r)$. Here, $u(r)$ is the Lennard–Jones attractive perturbation potential [se eq. (3.4)]. For all three states the temperature is $k_BT/\varepsilon = 1.15$. The densities are $\rho d^3 = 0$ 0.5, and 0.85.

This is analogous to Mayer's result, except that we have used a differen form of the renormalized potential. In this renormalized potential, the direc interaction between two molecules is canceled to some extent by the additio of other diagrams, this cancellation being more effective at high density tha at low density. Moreover, the fact that the entire cluster series can be ex pressed in terms of $C_L(r)$ indicates that this cancellation occurs systematicall throughout the cluster series. Thus, this new series is in effect an expansio in powers of the renormalized potential and of the density, and for model of simple liquids the expansion converges quickly if either the density or th renormalized potential (or both) is small. The arguments given above and th numerical results presented below indicate that the renormalized potentia is small if either the temperature is high or the density is large. Thus th series converges well at high density, at low density, and at high temperatur For any particular potential, however, it is necessary to perform explici calculations to determine more precisely the conditions under which th renormalized potential is small and the series converges quickly.

If the terms in (4.37) decrease in magnitude quickly enough, we can discar all but the first term to get

$$\ln g(r) = \ln g_d(r) + C_L(r) \tag{4.3}$$

or

$$g(r) = g_d(r)e^{C_L(r)} \tag{4.3}$$

This is called the exponential (EXP) approximation and its accuracy for various fluids has been tested. Some of the results will be reviewed below.

E. Comments on the New Renormalization Technique

This new renormalization technique has many of the same features and justifications as did Mayer's. Here again we do not know how to relate the physical nature of the (repulsive force) screening effect to the topological structure of the diagrams included in C_L. However, the structure of the C_L diagrams, namely chains of h_d and ϕ bonds "decorated" with additional f_d bonds, suggest the following interpretation. Screening of a perturbation potential occurs even for non-Coulombic potentials and is accounted for approximately by summing chains of interactions. In dense liquids, the screening represents a competition between attractive and repulsive interactions, and so h_d bonds, representing the repulsions, must be included as links in the chains, as well as the ϕ bonds. For short-ranged perturbations, the field points in the chains are constrained to be close to one another—so close that nonadjacent members may come within a hard core distance of one another. This is physically impossible but is mathematically allowable in cluster integrals. To correct for the hard core interactions between points in the chain, we should include some diagrams in which these points are connected by f_d bonds.

As in Mayer's theory, our choice of renormalized potential can be justified only with mathematical and experimental reasons. We have seen that this choice eliminates the divergences in the chain sum and that the renormalized potential can be used to eliminate the original potential from the cluster series. We also will see below that the simplest approximation suggested by the theory, the exponential approximation, is in very good agreement with computer experiments on simple liquids. It is also accurate for ionic solutions.[47,48] The present choice of renormalized potential is certainly not unique. It is possible to make at least one other choice (see Appendix B) which retains desirable features of the present choice (but which does not lead to significantly different results), and there may be other choices which are better for a wider variety of liquids. The choice we have made, however, is certainly adequate for a treatment of simple liquids and ionic solutions.

F. Principal Results of the Renormalized Cluster Theory

The most important results of the preceding discussion are (4.37) and (4.39) for the pair correlation function of a fluid of attracting hard spheres. The former is an exact formal result; the latter is a truncation of the infinite series and represents a useful and tractable numerical approximation. The same type of renormalization methods can be applied to an analysis of the cluster series for the excess free energy density of such a fluid. An infinite series can be

obtained in which all the diagrams are expressed in terms of the renormalized potential C_L. The reader is referred to Ref. 5 for the details. When the series is truncated the result is

$$\mathscr{A} = \mathscr{A}_d + a_{\text{HTA}} + a_{\text{ORPA}} + B_2 \tag{4.40}$$

where $\mathscr{A}_d$ is the hard sphere excess free energy density,

$$a_{\text{HTA}} = -\frac{\beta}{2}\rho^2 \int \mathbf{dr}\, g_d(r)u(r) \tag{4.41}$$

$$a_{\text{ORPA}} = -\frac{1}{2(2\pi)^3}\int \mathbf{dk}\{\rho\hat{\phi}(k)\hat{S}_d(k) + \ln\,[1 - \rho\hat{\phi}(k)\hat{S}_d(k)]\} \tag{4.42}$$

$$B_2 = \frac{1}{2}\rho^2 \int \mathbf{dr}\, h_d(r)\frac{1}{2}\,[C_L(r)]^2 + \frac{1}{2}\rho^2 \int \mathbf{dr}\, g_d(r)\sum_{n=3}^{\infty}(n!)^{-1}[C_L(r)]^n \tag{4.43}$$

Equation (4.40) is called the ORPA + B_2 approximation for historical reasons.

The conditions under which (4.40) is an accurate approximation for the entire cluster series are approximately the same as the conditions for the validity of (4.39). These results were originally derived in a somewhat different way[5] and are collectively referred to as the optimized cluster theory.

G. Tests of Optimized Cluster Theory

This theory for calculating the structural and thermodynamic properties of a fluid from its interatomic potential has been applied to a variety of potentials, such as the Lennard–Jones potential, primitive models of electrolyte solutions, and the square well potential. In this section we discuss tests of this theory for the Lennard–Jones potential described above in Section III.

The Lennard–Jones potential has a soft repulsive core rather than a hard sphere interaction. However, the optimized cluster theory results can easily be modified to take the softness into account, using the methods discussed in Section II. The details of the derivation will be omitted. The results are

$$g(r) = e^{-\beta[u_0(r)+u(r)]}y_d(r)e^{[C_L(r)-\Phi(r)]} \tag{4.44}$$

which is analogous to (4.39) and (2.16), and

$$\mathscr{A} = \mathscr{A}_d + a_{\text{HTA}} + a_{\text{ORPA}} + B_2 \tag{4.45}$$

In (4.44) and (4.45) the renormalized potential is the one calculated for a fluid whose potential is a hard core with diameter d plus the attractive part of the original potential. In (4.44), the function $C_L(r) - \Phi(r)$ for $r < d$ is to be interpreted as the smooth extrapolation of its functional behavior for $r > d$.

The hard sphere diameter should be chosen so that

$$\int \mathbf{dr}[e^{-\beta u_0(r)} - e^{-\beta u_d(r)}]y_d(r)e^{[C_L(r)-\Phi(r)]} = 0 \tag{4.46}$$

However, in practice for potentials like the Lennard–Jones potential, $C_L(r) - \Phi(r)$ is slowly varying compared to $y_d(r)$ near $r = d$ and therefore it is adequate to use the diameter calculated from the simpler criterion in (2.11).

There are two types of unambiguous tests to which we can subject these results. First, we can compare the thermodynamic properties and the pair correlation function with molecular dynamics and Monte Carlo calculations for the Lennard–Jones fluid. Secondly, we can test the theory for internal consistency.

The first type of test is made in Table II and Figs. 14 and 15, which compares the OCT with computer simulation results. It can be seen that throughout the temperature–density plane the agreement is excellent and that the discrepancy between the OCT and computer simulation results are usually of the same magnitude as the statistical uncertainties of the latter.

The second type of test can be carried out by calculating the pressure (or the internal energy) in two ways. The first way is to calculate the excess free energy from (4.45) and then differentiate numerically with respect to density to obtain the pressure (or with respect to temperature to obtain the internal energy). The second way is to use the virial equation (or the

TABLE II

Pressure and Internal Energy for the Lennard–Jones Fluid Calculated Using the ORPA + B_2 Approximation of the Optimized Cluster Theory (OCT) Compared with the Results Computed from the High-Temperature Approximation (HTA) and from Monte Carlo Computer Simulations (MC)

		$\beta P/\rho$			$-\Delta E/N\epsilon$		
$\rho\sigma^3$	$k_B T/\epsilon$	HTA[a]	OCT[b]	MC[c]	HTA[a]	OCT[b]	MC[c]
0.1	0.75	0.42	0.23	0.23	0.56	1.15	1.15
0.1	1.35	0.77	0.72	0.72	0.55	0.78	0.78
0.2	1.35	0.53	0.50	0.51	1.16	1.51	1.50
0.5	1.35	0.18	0.30	0.30	3.24	3.36	3.37
0.65	1.15	0.13	0.22	0.31	4.41	4.47	4.45
0.85	1.15	2.85	2.84	2.86	5.66	5.69	5.67

[a] Obtained by numerical differentiation of (3.8).

[b] Obtained by numerical differentiation of (4.45).

[c] Machine calculation results taken from Verlet and Weis.[10] The uncertainty in these results at high densities is ± 0.05.

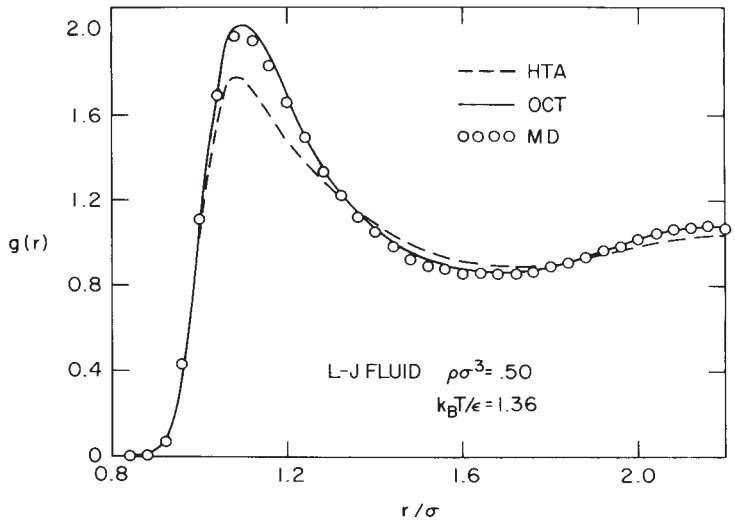

Fig. 14. Pair correlation function for the Lennard–Jones fluid for a state near the critical point. The open circles ar the molecular dynamics results of Verlet.[9] The dashed and solid curves are the results of the high-temperature approximation and the optimized cluster theory, respectively.

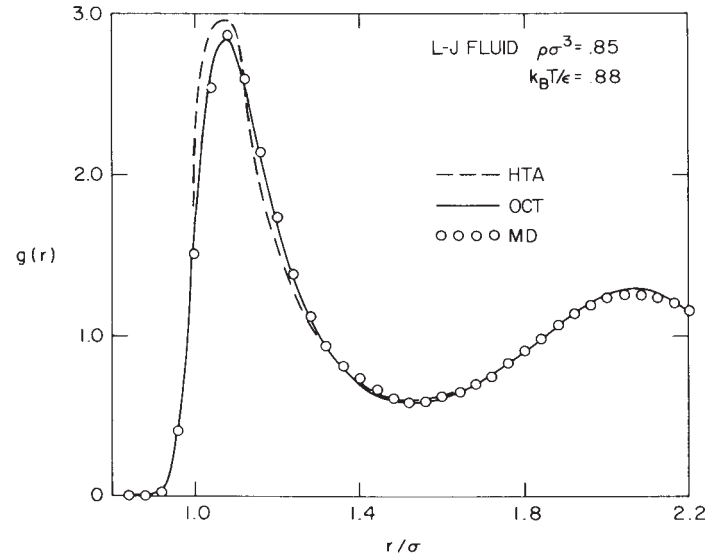

Fig. 15. Pair correlation function for the Lennard–Jones fluid for a state near the triple point. See Fig. 14 for additional information.

energy equation) and the exponential approximation for the pair correlation function to obtain the pressure (or the internal energy). Comparison of the two results gives a measure of the internal consistency and hence of the accuracy of the theory. There is no reason to expect that the two theoretical results for the pressure should contain errors that are consistently equal to each other, and this is why agreement between them is a measure of the accuracy of each. In fact there is good reason to expect that the errors of the two results are very different in magnitude. The expansion parameters in the cluster series for $\mathscr{A}$ and g are ρR^3 and $\bar{C}$, where R and $\bar{C}$ are the range and average magnitude of the renormalized potential, respectively. The cluster series corrections to the ORPA + B_2 approximation for $\mathscr{A}$ are of order $\rho(\rho R^3)^2(\bar{C})^2$, whereas the corrections to the EXP approximation are of order $\rho R^3\bar{C}$. It follows that the compressibility factor calculated from the ORPA + B_2 approximation contains errors of order $(\rho R^3)^2\bar{C}^2$, whereas the virial compressibility factor from EXP has errors of order $\rho R^3\bar{C}$. Thus the differences between them are of order $\rho R^3\bar{C}$. If the differences are found to be small, then the expansion parameters are small and the OCT approximations are accurate.

The entries in Table III show how well the OCT satisfies the consistency test for the Lennard-Jones fluid at several representative states. At high densities ($\rho\sigma^3 > 0.65$) the differences between the compressibility factors

TABLE III

Comparison of the Compressibility Factors of the Lennard-Jones Fluid as Calculated by Differentiating the ORPA + B_2 Approximation ($\beta P_f/\rho$) and by Applying the Virial Equation to the EXP Approximation ($\beta P_v/\rho$)

$\rho\sigma^3$	$k_B T/\epsilon$	$\beta P_f/\rho$	$\beta P_v/\rho$
0.154	1.351	0.60	0.60
0.107[b]	1.249[b]	0.65	0.66
0.318[a]	1.303[a]	0.30	0.28
0.558[b]	1.249[b]	0.17	0.18
0.748	1.351	1.67	1.70
0.757	1.249	1.52	1.54

[a] This state is the "experimental" critical point for the Lennard-Jones fluid.[49] At that state the experimental compressibility factor is 0.29.

[b] This state is in the critical region and directly adjacent to the liquid-gas coexistence curve.[49] See Fig. 1.

calculated by the two methods differ by no more than 0.03. A difference of this magnitude is expected because of the uncertainty in our knowledge of the hard sphere equation of state and of $g_d(r)$, both of which are used as input for the OCT. At lower densities, however, these quantities are known more accurately, and any differences larger than 0.01 are significant. At low and moderate densities, differences of this size are found only for states very close to the liquid-gas critical point. The failure of the OCT to satisfy the consistency test near the critical point is one manifestation of the fact that OCT provides a classical theory of phase transitions. A detailed study of the predictions of the OCT in the vicinity of the liquid-gas phase transition has been reported by Sung and Chandler.[49]

H. Concluding Remarks

The optimized cluster theory has been applied to the study of various types of liquids, namely the Lennard–Jones fluid,[47] ionic solutions,[47] and mixtures of hard spheres and square well molecules.[50] A generalization of the theory has been applied to water (D. Chandler and H. C. Andersen, unpublished) and to fused salts (S. Hudson and H. C. Andersen, unpublished). These calculations have met with varying degrees of success. For the first group of fluids, the accuracy of the theory is remarkably good. However for the last two types of fluids, the accuracy is very poor and the OCT is qualitatively incorrect as a description of these fluids.

From the derivation of the EXP and ORPA + B_2 approximations, one would expect them to be accurate whenever the product of ρR^3 and $\bar{C}$ is small. Here $\bar{C}$ and R are the strength and range of the renormalized potential. In all the cases tested, this was found to be a valid indicator of the accuracy of the theory. It follows that EXP and ORPA + B_2 are accurate whenever the perturbation is causing a relatively small change in the number of nearest neighbors of a molecule and in the overall distribution of molecules around a given molecule.* Moreover, the results of an OCT calculation (namely the strength and range of the calculated renormalized potential as well as the consistency check) provide a clear indication of how much to trust the ORPA + B_2 and EXP approximations for any particular fluid.

V. IMPLICATIONS

The results discussed in Sections III and IV for the structure of the Lennard–Jones liquid at high density are special cases of more general principles that may be applicable to liquids.

* An OCT calculation requires that the potential be separated into a reference part plus a perturbation. Only the perturbation is treated using the renormalization technique. For the fluids mentioned above for which OCT gave poor results, it might be true that a different separation of the potential would improve the accuracy of the results.

We have seen that the attractive part of the Lennard–Jones potential is not small compared with $k_B T$ at liquid temperatures, yet it has only a small effect on the structure of the liquid compared with the overwhelming effect of the short-ranged repulsions. We believe it is generally true that at high density the short-ranged repulsions are dominant and the effect of attractions is small; this principle applies to molecular as well as atomic liquids and to some nonequilibrium properties as well as to the equilibrium structure.

This idea means that at high densities the static and dynamic structures of a dense liquid are determined mainly by the shape of the molecules that comprise the fluid. We have shown that when the molecular shape is spherical (or nearly spherical) and if the hard sphere diameter is chosen properly, the static structure due to continuous short-ranged repulsions is related very simply to that of a hard sphere fluid at the same density. We believe that the dynamic as well as static properties of repulsive force systems are close to those in an appropriately chosen hard sphere system. Thus, for dense liquids composed of fairly spherical molecules, the motion of molecules in the fluid should be related simply to the particle motion in a model hard sphere fluid. Similarly, we expect that the static and dynamic properties of dense fluids of molecules that are approximately ellipsoidal in shape (or tetrahedral, or rod-like, etc.) should be simply related to those of model fluids of hard ellipsoids (or hard tetrahedra, or hard rods, etc).

In this section we will outline some of the available evidence for the validity of these ideas. Further, we will discuss reasons for possible exceptions to these principles.

A. Equilibrium Structure of Molecular Liquids

There is a growing amount of evidence to support the belief that the intermolecular correlations in dense molecular fluids are determined by the shape of the molecules in the fluid. Sung and Chandler[28] showed that repulsive forces dominate the center of mass radial distribution function determined by Berne and Harp from molecular dynamics computations on a model for liquids composed of diatomic molecules. Lowden and Chandler[51,52] have studied the intermolecular equilibrium correlations in molecular liquids for which the molecules are assumed to be composed of overlapping hard spheres which are fused together rigidly. The fluid structure for these nonspherical hard core models is obviously due to steric effects and nothing else. The calculations by Lowden and Chandler show that these steric effects produce the measured features of the intermolecular structures of the following liquids: N_2, CS_2, CSe_2, C_6H_6, and CCl_4.

There is no evidence that dipole–dipole (or quadrupole–quadrupole, etc.) terms in intermolecular potentials are significant in determining the

microscopic intermolecular correlations in real one-component dense fluids.* These terms in the multipole expansion for interactions describe the slowly varying forces between molecules at large intermolecular separations. From the discussion presented in the Introduction, and from the calculations presented in Sections III and IV, one expects that slowly varying portions of intermolecular potentials play only a small role in determining the liquid structure.

B. Freezing

The concept that the harshly repulsive parts of the intermolecular forces determine the structure of a dense fluid leads naturally to the idea that excluded volume effects (and not attractive forces) are chiefly responsible for the liquid–solid freezing transition. This idea was used by Longuet-Higgins and Widom[6] when they developed a theory for the freezing of liquid argon. Their work, and that of others,[54,55] indicates that the freezing transition in simple fluids is intimately related to the fluid–solid transition that occurs in a hard sphere system.[56] Although the numerical values of the thermodynamic properties associated with the transition (e.g., heat of fusion, density discontinuities) do depend on attractive forces, the mechanism for freezing in simple fluids is the same instability in the fluid phase which causes the hard sphere to solidify at high densities.

C. Two Causes for Exceptions

When attractive forces do produce a significant structural effect in a dense fluid, the reason for it is easy to understand. The effect of hydrogen bonds in liquid water is one example already mentioned in the Introduction. The structure of some liquid mixtures provides another example. In this case, it is possible for the attractive interactions to produce structural effects which need not compete with the role of the repulsive forces. This point is illustrated most simply by the model system composed of hard spheres of diameter σ mixed with a square well species with the same hard core diameter and an attractive well of range 1.5 σ.[57] The attractions between the square wells tend to make the square well particles cluster together. This clustering can occur without changing the excluded volume correlations produced by the hard cores. As a result, the attractions are able to create important structural effects.

* However, the long-ranged nature of dipole–dipole interactions create a many-body cooperative phenomenon which significantly effects the long-range *asymptotic* decay of pair correlations. Indeed, for many-body systems containing dipoles, the asymptotic behavior of the pair correlations depend on the shape of the container of the macroscopic system. A review covering this subject is given by Deutch.[53]

Thus, there are two possible situations in which attractive interactions can play a significant role in determining the intermolecular correlations of dense fluids. In one, relevant to liquid water, the attractive forces are sufficiently large and quickly varying so that they can actually rupture the structure formed by the repulsive forces. When this situation occurs, the optimized cluster theory discussed in Section IV cannot describe the effects of the attractions.* In the other situation, which is frequently important for liquid mixtures, the attractive interactions can produce structural effects provided they do not compete with the correlations produced by the repulsions. For this latter case, it appears that the optimized cluster theory can successfully describe the effects of the attractions.[50,57]

D. Liquid Crystals

When molecules in a fluid are very long, the fluid can exist as a liquid crystal as well as an isotropic liquid. A rough estimate of the dimensions of a typical liquid crystal molecule [e.g., MBBA (*p*-methyloxybenzylidene-*n*-butylaniline) is approximately a spherocylinder 20 Å in length and 5 to 6 Å in width] shows that at liquid crystal densities (for MBBA at 1 atm pressure, $\rho \approx 2.3 \times 10^{-3}$ Å^{-3}), the molecules are indeed crushed extremely close to one another. As a result it is not likely that the dipole–dipole interactions, for example, are competitive with the harshly repulsive forces which define the shape of the molecules. The intermolecular structure of a liquid crystal is almost certainly determined by the long shape of the molecule. Indeed, this view is corroborated by recent light scattering measurements[59] of the Kirkwood g-factor as a function of density and temperature for the dense isotropic liquid phases of MBBA, MBA (*p*-methylbenzylidene-*n*-butylaniline) and EBA (ethylbenzylidene-*n*-butylaniline).

The expectation that the structure of a liquid crystal is determined mainly by the shape of the molecules in the fluid together with the current understanding of the liquid–solid phase transition for simple systems leads us to expect that the mechanism for the phase transition between isotropic fluid and liquid crystal phases should be understood in terms of the packing of long hard particles. Onsager[60] used this physical picture when developing his theory of the isotropic–anisotropic fluid phase transition. However, his

* It is possible that one can devise a statistical mechanical theory for a repulsive force system which exhibits the tetrahedral intermolecular structure that occurs in liquid water. If this repulsive force system is used as the reference system for liquid water, then the hydrogen bonds will not cause appreciable changes in the fluid structure, and the optimized cluster theory will probably provide a useful way of describing the effects of hydrogen bonds in liquid water. However, if the chosen reference system for water does not exhibit tetrahedral ordering, the hydrogen bonds will cause too great an effect to be calculated from a simple application of optimized cluster theory (H. C. Andersen and D. Chandler, unpublished work). Instead a new renormalization of the hydrogen bond is required.[58]

theory also employed severe mathematical approximations which have been shown to be inaccurate.[61] It is our belief that the approximations, and not the physical picture, are the source of some of the incorrect predictions of the theory.

Our conjecture about the mechanism for the transition between liquid crystal and isotropic liquid phases contradicts the physical picture used in many of the theories of liquid crystals.[62,63] These theories attribute the properties of liquid crystals to dipole–dipole interactions. All of the arguments we have presented suggest that this physical picture is incorrect.

E. Molecular Motion in Liquids

The work of Kushick and Berne[64] provides direct evidence that the dynamical processes occuring in dense liquids are governed primarily by the short-ranged repulsive forces. In that work, computer simulations were performed for both the Lennard–Jones reference systems and the Lennard–Jones fluid itself. By comparing the results obtained for both systems, Kushick and Berne showed that at high density the velocity autocorrelation function for the reference system is similar to that for the total Lennard–Jones liquid. The attractive forces indeed play a minor role.

If the molecules in a liquid are fairly spherical in shape, it seems reasonable that the dynamics produced by the repulsive forces should be close to that occurring in a hard sphere fluid. This idea was probably first used by Enskog (see e.g., Chapman and Cowling[65]). The theory of transport developed by Enskog and the modern developments of present-day researchers provide evidence that molecular motion in dense fluids composed of fairly spherical molecules is related simply to particle motion in the hard sphere fluid.

Verlet and coworkers[13,66] have shown that the diffusion constant of the Lennard–Jones fluid is represented to within 10% by the diffusion constant of the hard sphere fluid. The diameter was, in effect, chosen to be the one associated with $u_0(r)$ according to (2.11). Protopapas et al.[67] have used the hard sphere model to calculate diffusion constants for a wide variety of liquid metals.

The diffusion constant is the zero-frequency Fourier component of the velocity autocorrelation function. Thus the work of Verlet and of Protopapas et al. indicates that the zero-frequency components for a fluid with a realistic interatomic potential and for its associated hard sphere system are, to a good approximation, the same. Kim and Chandler[68,69] have used a similar assumption in their development of a qualitatively accurate phenomenological theory of the velocity autocorrelation function for simple liquids. Chandler[70] has used the apparent connection between dynamics due to continuous repulsive forces and the dynamics of hard sphere particles to develop a simple theory for rotational and translational motion in molecular

liquids. One of the principal results of this theory is a microscopic derivation of Gordon's J-diffusion model approximation.[71] The microscopic derivation allows one to arrive at these results without recourse to the unphysical assumptions usually attributed to Gordon's theory. Further, a useful expression is found for the relaxation time introduced phenomenologically by Gordon. Chandler[70] has shown that this expression predicts results that are in close agreement with those found from computer simulations on a model for liquid nitrogen.[72] The theory has also been used successfully to interpret high-pressure experiments which probe rotational and translational motions in liquids.[73–76]

F. Summary

There exists compelling evidence that at the high densities which characterize most of the liquid phase the dynamic and static structures of liquids are dominated by the short-ranged repulsive forces. It is our opinion that the phenomena that occur in most liquids are best understood by considering first the excluded volume effects produced by these forces. The attractive interactions and other slowly varying forces such as dipole–dipole interactions produce "second-order" effects which can usually be described by perturbation theory or ignored altogether. The application of this idea has produced the quantitative equilibrium theory of simple liquids discussed in this article. We believe subsequent applications will produce accurate theories for the dynamic and static correlations in complex molecular fluids.

APPENDIX A. SOME GRAPH THEORETIC TERMINOLOGY

In this appendix, we will give brief definitions of some of the graph theoretic terms used in the text. The graphs we are concerned with consist of points and bonds. The points represent particles are are of two types: root points (usually two of them are in a graph) and field points (any number of them may appear). There are various types of bonds, such as h_d, ϕ, C_L and f_d bonds. The bonds represent either interactions between the particles (e.g., ϕ or f_d) or correlations between the particles which are induced by the interactions (e.g., h_d or C_L).

A diagram is *connected* if it is possible to travel from any point to any other point along a path consisting of bonds and points. For example, in Fig. A-1, the first diagram is connected and the second is not.

Fig. A-1. Illustration of the definition of a connected diagram. The first diagram is connected and the second is not connected.

An *articulation point* is a root point or a field point which if removed would leave the diagram disconnected in such a way that at least one of the disconnected parts contains no root points. For example, the last two diagrams in Fig. A-2 have articulation points and the first one does not.

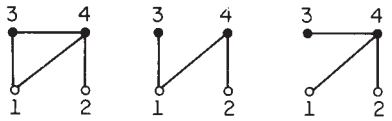

Fig. A–2. Illustration of the definition of articulation point. In the second diagram, point 1 is an articulation point. In the third, 4 is an articulation point. The first has no articulation points.

A *reference pair of articulation points* is a pair of points which if removed would disconnect the diagram in such a way that at least one of the disconnected parts contains no root point and one or more field points and only bonds that are related to the reference system (i.e., h_d and f_d bonds). For example, the last two diagrams in Fig. A-3 have a reference pair of articulation points.

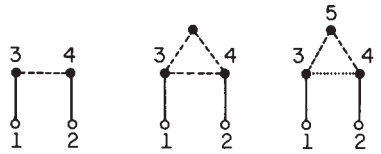

Fig. A–3. Illustration of the definition of a reference pair of articulation points. Here the dashed and dotted lines represent h_d and f_d bonds, respectively. These are reference system bonds. In the last two diagrams, points 3 and 4 are a reference pair of articulation points.

APPENDIX B. DIAGRAMATIC FORMULATION OF THE MEAN-SPHERICAL-MODEL INTEGRAL EQUATION

The mean-spherical-model (MSM) integral equation proposed by Lebowitz and Percus[77] has been the focus of great interest during the past few years. The solutions of this integral equation provide an approximation to $g(r)$ for classical fluids in which the pair interactions are of the form

$$\begin{aligned} w(1,2) &= \infty, & r_{12} &< d \\ &= u(1,2), & r_{12} &> d \end{aligned} \tag{B.1}$$

where $u(1, 2)$ is finite but otherwise arbitrary. It may, for example, depend on particle orientations as well as the separation between centers. The primary

reason for the interest in the MSM equation is that it is exactly soluble for several nontrivial systems.

When the perturbation interaction, $u(1, 2)$, is exactly zero, the system is the hard sphere fluid, and the MSM equation becomes the Percus–Yevick equation for hard spheres. Wertheim[22] and Theile[21] have presented the exact solutions for this case. Wertheim[78] has also solved the MSM equation when the perturbation is the dipole–dipole interaction. For that case the particles in the fluid are hard spheres with permanent electric dipoles. Other one-component fluids for which exact solutions have been derived are hard spheres with Yukawa potentials as the perturbation,[79] polarizable hard spheres with permanent electric dipoles,[80] and charged hard spheres in a uniform neutralizing background.[81] The two-component fluids for which solutions are available are the neutral mixture of charged hard spheres in a dielectric continuum,[82] hard spheres mixed with hard spheres containing permanent point dipoles,[83] and hard spheres with point dipoles mixed with charged hard spheres.[84–86] More general multipole-electrostatic interactions have also been studied.[87] In addition to the analytic solutions, the MSM equation has been applied numerically to study the structure of real liquids with differing degrees of success.[88–90]

In this appendix we will discuss the cluster–diagramatic formulation of the MSM equation. This formulation shows the close connection of the MSM equation to the OCT. Further, it reveals the strengths and limitations of theories which are based on this equation. As a result, one is able to judge *a priori* whether a particular application of the MSM equation will be successful.

For notational simplicity, we consider only one-component systems with spherically symmetric perturbations. The generalizations to many components and to $u(1, 2)$ functions that depend on orientations are straightforward. The MSM equation is the Ornstein–Zernike equation for $g(r) - 1 = h(r)$ (see Ref. 38*b*)

$$h(r) = c(r) + \rho \int \mathbf{dr}' c(|\mathbf{r} - \mathbf{r}'|)h(r') \tag{B.2}$$

plus the closure relations

$$h(r) = -1, \qquad r < d \tag{B.3}$$

and

$$c(r) = -\beta u(r), \qquad r > d \tag{B.4}$$

Equation (B.3) is exact for particles with a hard core. Equation (B.4) is the only approximation. The quantity $c(r)$, which is defined by (B.2), is called the

direct correlation function. By using Fourier transforms, (B.2) can be written as

$$\hat{h}(k) = \hat{c}(k)[1 - \rho\hat{c}(k)]^{-1} \tag{B.5}$$

Thus, one solves the MSM equation [(B.2), (B.3) and (B.4)] by finding the $c(r)$ for $r < d$ which makes $h(r) = -1$ inside the hard core. Then for $r > d$, $h(r)$ is determined by inverting (B.5).

The reader may notice the similarity between (B.5) and (4.15). The similarity implies that $h(r)$ is $c(r)$ plus the sum of all singly connected chains of two or more c functions. (This can be checked by solving (B.2) iteratively with ρ as the ordering parameter.) As a result we have the exact result that[38b,c]

$$c(r) = \text{sum of all nodeless diagrams in } h(r) \tag{B.6}$$

It is possible to find a subset of these nodeless diagrams which can be summed to form $c_{\text{MSM}}(r)$, the direct correlation function in the MSM approximation. To do this it is convenient to consider a class of diagrams which are similar to those used in Section IV to construct $C_L(r)$ (see Fig. 10). Imagine a polygon with three or more vertices. Make two adjacent vertices the root points; the remaining ones are the field points. Connect each pair of adjacent points with either a f_d bond or a Φ bond (but not both), except that no such bond is to connect the roots directly. (Here, $f_d(r)$ is the hard sphere Mayer cluster function, and $\Phi(r) = (1 + f_d)(-\beta u)$. Thus, $\Phi(r)$ is $-\beta u(r)$ for $r > d$, and it is zero for $r < d$.) Next, add some or no f_d bonds between nonadjacent vertices in such a way that no two f_d bonds cross. There are no other restrictions. Let $D(r)$ denote the sum of all such diagrams. Then the following equalities can be proven by straightforward topological considerations:

$$h_{\text{MSM}}(r) = f_d(r) + \Phi(r) + [1 + f_d(r)]D(r) \tag{B.7}$$

and

$$c_{\text{MSM}}(r) = f_d(r) + \Phi(r) + f_d(r)D(r) \tag{B.8}$$

To verify these results one must do three things. First, note that the right-hand side of (B.7) satisfies (B.3). Second, note that the right-hand side of (B.8) satisfies (B.4). Third, show that (B.7) and (B.8) satisfy (B.2). This is done by using the definition of $D(r)$ to establish that $c_{\text{MSM}}(r)$ does contain all the nodeless diagrams in $h_{\text{MSM}}(r)$ and that all the diagrams (and no more) contained in $h_{\text{MSM}}(r)$ are generated by summing all the singly connected chains of c_{MSM} bonds.

One may extract from $h_{\text{MSM}}(r)$ all the diagrams containing no Φ bonds. The sum of these diagrams is the Percus–Yevick correlation function for hard spheres,[46] $h_d^{(\text{PY})}(r)$. By a topological reduction,[38c] the remaining diagrams in

$h_{MSM}(r)$ (those involving one or more Φ bonds) may be expressed in terms of Φ, f_d, and $h_d^{(PY)}$ bonds. The result is

$$h_{MSM}(r) - h_d^{(PY)}(r) = \Phi(r) + [1 + f_d(r)][\text{sum of all diagrams formed in the same way as those in } D(r) \text{ except now on the exterior of the polygon we have } h_d^{(PY)} \text{ instead of } f_d \text{ bonds, and no diagram is permitted if any field point in the diagram is intersected by only } h_d^{(PY)} \text{ bonds}] \tag{B.9}$$

By comparing (B.9) with the definition of $C_L(r)$ given in Section IV, we see that

$$h_{MSM}(r) = h_d^{(PY)}(r) + C_L^{(PY)}(r) \tag{B.10}$$

where $C_L^{(PY)}(r)$ is $C_L(r)$ evaluated using the Percus–Yevick approximation for h_d rather than the exact hard sphere correlation function. Equation (B.10) has been derived before using a very different method.[5]

There are two important points that can be drawn from this analysis. First, since the Percus–Yevick theory is fairly accurate for hard spheres, there is only a small difference between $C_L^{(PY)}(r)$ and $C_L(r)$. Therefore, one may use the analytic solution of the MSM equation (if it is obtainable) to calculate

$$C_L(r) \cong h_{MSM}(r) - h_d^{(PY)}(r) \tag{B.10}$$

One may then use this analytic expression to calculate $g(r)$ from the OCT (in particular, the EXP approximation):

$$g(r) \cong g_d(r) \exp [h_{MSM}(r) - h_d^{(PY)}(r)] \tag{B.11}$$

Equation (B.11) is inherently more accurate than $g_{MSM}(r) \cong g(r)$.[47] However, its accuracy is limited, and this brings us to the second point. As discussed in Section IV, the OCT is accurate only if $\rho C_L(r)$ is small. Thus, (B.11) and the MSM equation even more so are accurate and thus useful only when the quantity $\rho[h_{MSM}(r) - h_d^{(PY)}(r)]$ is small. The MSM equation is not reliable if the equation predicts that the fluid structure is significantly different from that of the hard sphere system. Thus, whenever the structural properties of a fluid are qualitatively different from those of the noble gas fluids the MSM cannot be expected to give even a qualitatively correct description. For example, the MSM will not provide a correct theory for liquid water or for fused salts. Further, the MSM equation will not be accurate if an unsatisfactory division is made of the pair potential (see Section III). The reference potential must be harsh enough that its effects are nearly those of

a hard core with diameter d; and the reference potential must contain all the quickly varying repulsive interations. If these conditions are not met, $\rho[h_{\mathrm{MSM}}(r) - h_d^{(\mathrm{PY})}(r)]$ will not be small.

Acknowledgments

We are grateful to Stephen H. Sung for providing us with his unpublished numerical results for the Lennard–Jones fluid. The information depicted in Fig. 4, and some of the entries in Tables II and III were obtained from his unpublished calculations. We also want to thank George Stell for helpful comments on a previous version of this paper.

This work was supported in part by grants from the National Science Foundation (GP 20058A and MPS 73–08591 A02), the Petroleum Research Fund as administered by the American Chemical Society, and the Alfred P. Sloan Foundation.

References

1. D. Chandler and J. D. Weeks, *Phys. Rev. Lett.*, **25**, 149 (1970).
2. J. D. Weeks, D. Chandler, and H. C. Andersen, *J. Chem. Phys.*, **54**, 5237 (1971).
3. *Ibid.*, **55**, 5421 (1971).
4. H. C. Andersen, J. D. Weeks, and D. Chandler, *Phys. Rev.*, **A4**, 1597 (1971).
5. H. C. Andersen and D. Chandler, *J. Chem. Phys.*, **57**, 1918 (1972).
6. H. C. Longuet-Higgens and B. Widom, *Mol. Phys.*, **8**, 549 (1964).
7. H. Reiss, *Adv. Chem. Phys.*, **IX**, 1 (1965).
8. J. A. Barker and D. Henderson, *J. Chem. Phys.*, **47**, 4714 (1967).
9. L. Verlet, *Phys. Rev.*, **165**, 201 (1968).
10. L. Verlet and J. J. Weis, *Phys. Rev.*, **A5**, 939 (1972).
11. J. A. Barker and D. Henderson, *Ann. Rev. Phys. Chem.*, **23**, 439 (1972).
12. H. C. Andersen, *Ann. Rev. Phys. Chem.* **26**, 145 (1975).
13. L. L. Lee and D. Levesque, *Mol. Phys.*, **26**, 1351 (1973).
14. W. A. Steele and S. I. Sandler, *J. Chem. Phys.*, **61**, 1315 (1974).
15. S. I. Sandler, A. D. Gupta, and W. A. Steele, *J. Chem. Phys.*, **61**, 1326 (1974).
16. M. H. Kalos, D. Levesque, and L. Verlet, *Phys. Rev.*, **A9**, 2178 (1974).
17. D. Shiff, *Nature*, **243**, 130 (1973).
18. G. Stell, J. C. Rasaiah, and H. Narang, *Mol. Phys.*, **27**, 1393 (1974).
19. B. J. Alder and T. E. Wainwright, *J. Chem. Phys.*, **33**, 1439 (1960).
20. J. K. Percus and G. J. Yevick, *Phys. Rev.*, **110**, 1 (1958).
21. E. Thiele, *J. Chem. Phys.*, **39**, 474 (1963).
22. M. S. Wertheim, *Phys. Rev. Lett.*, **10**, 321 (1963).
23. L. Verlet and J. J. Weis, *Mol. Phys.*, **24**, 1013 (1972).
24. J. A. Barker, *Proc. Roy. Soc. London*, **A241**, 547 (1957).
25. K. E. Gubbins, W. R. Smith, M. K. Tham, and E. W. Tiepel, *Mol. Phys.*, **22**, 1089 (1971).
26. T. L. Hill, *Statistical Mechanics*, McGraw Hill, New York, 1956.
27. J. P. Hansen and J. J. Weis, *Mol. Phys.*, **23**, 853 (1972).
28. S. H. Sung and D. Chandler, *J. Chem. Phys.*, **56**, 4989 (1972).
29. L. Verlet, *Phys. Rev.*, **159**, 98 (1967).
30. D. Levesque and L. Verlet, *Phys. Rev.*, **182**, 307 (1969).
31. R. Zwanzig, *J. Chem. Phys.*, **22**, 1420 (1954).
32. L. D. Landau and E. M. Lifshitz, *Statistical Physics*, Pergamon Press, London, 1958.
33. D. A. McQuarrie and J. L. Katz, *J. Chem. Phys.*, **44**, 2393 (1966).
34. B. Widom, *Science*, **157**, 375 (1967).
35. J. L. Lebowitz and O. Penrose, *J. Math. Phys.*, **7**, 98 (1966).

36. P. Debye and E. Hückel, *Physik Z.*, **24**, 185 (1923).
37. J. E. Mayer, *J. Chem. Phys.*, **18**, 1426 (1950).
38. Useful references on cluster theory include (*a*) H. J. Friedman, *Ionic Solution Theory*, Interscience, New York, 1962; (*b*) G. Stell in *The Equilibrium Theory of Classical Fluids*, H. L. Frisch and J. L. Lebowitz, Eds., Benjamin, New York, 1964; and (*c*) T. Morita and K. Hiroika, *Progr. Theor. Phys.*, **25**, 537 (1961).
39. J. L. Lebowitz, G. Stell, and S. Baer, *J. Math. Phys.*, **6**, 1282 (1965).
40. G. Stell, J. L. Lebowitz, S. Baer, and W. Theumann, *J. Math. Phys.*, **7**, 1532 (1966).
41. G. Stell and J. L. Lebowitz, *J. Chem. Phys.*, **49**, 3706 (1968).
42. P. Hemmer, *J. Math. Phys.*, **5**, 75 (1964).
43. G. Stell and K. Theumann, *Phys. Rev.*, **186**, 581 (1969).
44. G. Stell, *Phys. Rev.*, **184**, 135 (1969).
45. G. Stell, in *Phase Transitions and Critical Phenomena*, V. 5, C. Domb and M. S. Green, Eds., Academic, London, 1974.
46. G. Stell, *Physica*, **29**, 517 (1963).
47. H. C. Andersen, D. Chandler, and J. D. Weeks, *J. Chem. Phys.*, **57**, 2626 (1972).
48. S. Hudson and H. S. Andersen, *J. Chem. Phys.*, **60**, 2188 (1974).
49. S. H. Sung and D. Chandler, *Phys. Rev.*, **A9**, 1688 (1974).
50. S. H. Sung, D. Chandler, and B. J. Alder, *J. Chem. Phys.*, **61**, 932 (1974).
51. L. J. Lowden and D.Chandler, *J. Chem. Phys.*, **59**, 6587 (1973).
52. *Ibid.*, **61**, 5228 (1974).
53. J. M. Deutch, *Ann. Rev. Phys. Chem.*, **24**, 301 (1973).
54. J. J. Weiss, *Mol. Phys.*, **28**, 187 (1974).
55. R. K. Crawford, *J. Chem. Phys.*, **60**, 2169 (1974).
56. W. G. Hoover and F. H. Ree, *J. Chem. Phys.*, **49**, 3609 (1968).
57. B. J. Alder, W. W. Alley, and M. Rigby, *Physica*, **73**, 143 (1974).
58. H. C. Andersen, *J. Chem. Phys.*, **59**, 4714 (1973); *ibid.*, **61**, 4985 (1975).
59. G. R. Alms, T. D. Gierke, and W. H. Flygare, *J. Chem. Phys.*, **61**, 4083 (1974).
60. L. Onsager, *Ann. N.Y. Acad. Sci.*, **51**, (1949).
61. J. Vieillard-Baron, *Mol. Phys.*, **28**, 809 (1974).
62. G. Meier and A. Saupe, in *Liquid Crystals*, G. H. Brown, G. L. Dienes, and M. M. Labes, Eds., Gordon & Breach, London, 1966.
63. W. L. McMillan, *Phys. Rev.*, **A4**, 1238 (1971).
64. J. Kushick and B. J. Berne, *J. Chem. Phys.*, **59**, 3732 (1973).
65. S. Chapman and F. G. Cowling, *The Mathematical Theory of Non-Uniform Gases*, 3rd ed., Cambridge University Press, Cambridge, 1970.
66. D. Levesque and L. Verlet, *Phys. Rev.*, **A2**, 2514 (1970).
67. P. Protopapas, H. C. Andersen, and N. A. D. Parlee, *J. Chem. Phys.*, **59**, 15 (1973).
68. K. Kim and D. Chandler, *J. Chem. Phys.*, **59**, 5215 (1973).
69. D. Chandler, *Acc. Chem. Res.*, **7**, 246 (1974).
70. D. Chandler, *J. Chem. Phys.*, **60**, 3500, 3508 (1974).
71. R. G. Gordon, *J. Chem. Phys.*, **44**, 1830 (1966).
72. J. Barojas, D. Levesque, and B. Quentrec, *Phys. Rev.*, **A7**, 1092 (1973).
73. J. DeZwaan, R. J. Finney, and J. Jonas, *J. Chem. Phys.*, **60**, 3223 (1974).
74. J. DeZwaan and J. Jonas, *J. Chem. Phys.*, **62**, 4036 (1975).
75. J. H. Campbell, J. F. Fisher, and J. Jonas, *J. Chem. Phys.*, **61**, 346 (1974).
76. D. Chandler, *J. Chem. Phys.*, **62**, 1350 (1975).
77. J. L. Lebowitz and J. K. Percus, *Phys. Rev.*, **144**, 251 (1966).
78. M. S. Wertheim, *J. Chem. Phys.*, **55**, 4291 (1971).
79. E. Waisman, *Mol. Phys.*, **25**, 45 (1973).
80. M. S. Wertheim, *Mol. Phys.*, **26**, 1425 (1973).

81. R. G. Palmer and J. D. Weeks, *J. Chem. Phys.*, **58**, 4171 (1973).
82. E. Waisman and J. L. Lebowitz, *J. Chem. Phys.*, **56**, 3086, 3094 (1972).
83. S. A. Adelman and J. M. Deutch, *J. Chem. Phys.*, **59**, 3971 (1973).
84. *Ibid.*, **60**, 3935 (1974).
85. L. Blum, *Chem. Phys. Lett.*, **26**, 200 (1974).
86. L. Blum, *J. Chem. Phys.*, **61**, 2129 (1974).
87. *Ibid.*, **57**, 1862 (1972); **58**, 3295 (1973).
88. L. Blum and A. H. Narten, *J. Chem. Phys.*, **56**, 5197 (1972).
89. R. O. Watts, D. Henderson, and J. A. Barker, *J. Chem. Phys.*, **57**, 5991 (1972).
90. A. H. Narten, L. Blum, and R. H. Fowler, *J. Chem. Phys.*, **60**, 3378 (1974).